Terminal zone glacial sediment transfer at a temperate overdeepened glacier system

D.A. Swift [a, *], S.J. Cook [b], D.J. Graham [c], N.G. Midgley [d], A.E. Fallick [e], R. Storrar [f], M. Toubes Rodrigo [g], D.J.A. Evans [h]

[a] Department of Geography, University of Sheffield, Winter Street, Sheffield, S10 2TN, UK
[b] Geography, School of Social Sciences, University of Dundee, Nethergate, Dundee DD1 4HN, UK
[c] Polar and Alpine Research Centre, Department of Geography, Loughborough University, Leicestershire, LE11 3TU, UK
[d] School of Animal, Rural and Environmental Sciences, Nottingham Trent University, Nottinghamshire, NG25 0QF, UK
[e] Scottish Universities Environmental Research Centre, East Kilbride, Glasgow G75 0QF, UK
[f] Department of the Natural and Built Environment, Sheffield Hallam University, Howard Street, Sheffield S1 1WB, UK
[g] School of Science and the Environment, Manchester Metropolitan University, Manchester M1 5GD, UK
[h] Department of Geography, Durham University, South Road, Durham DH1 3LE, UK

ARTICLE INFO

ABSTRACT

Continuity of sediment transfer through glacial systems is essential to maintain subglacial bedrock erosion, yet transfer at temperate glaciers with overdeepened beds, where subglacial fluvial sediment transport should be greatly limited by adverse slopes, remains poorly understood. Complex multiple transfer processes in temperate overdeepened systems has been indicated by the presence of large frontal moraine systems, supraglacial debris of mixed transport origin, thick basal ice sequences, and englacial thrusts and eskers. At Svínafellsjökull, thrusts comprising decimetre-thick debris-rich bands of stratified facies ice of basal origin, with a coarser size distribution and higher clast content than that observed in basal ice layers, contribute substantially to the transfer of subglacial material in the terminal zone. Entrainment and transfer of material occurs by simple shear along the upper surface of bands and by strain-induced deformation of stratified and firnified glacier ice below. Thrust material includes rounded and well-rounded clasts that are also striated, indicating that fluvial bedload is deposited as subglacial channels approach the overdeepening and then entrained along thrusts. Substantial transfer also occurs within basal ice, with facies type and debris content dependent on the hydrological connectedness of the adverse slope. A process model of transfer at glaciers with terminal overdeepenings is proposed, in which the geometry of the overdeepening influences spatial patterns of ice deformation, hydrology, and basal ice formation. We conclude that the significance of thrusting in maintaining sediment transfer continuity has likely been overlooked by glacier sediment budgets and glacial landscape evolution studies.

© 2017 The Authors. Published by Elsevier Ltd. This is an open access article under the CC BY-NC-ND license (http://creativecommons.org/licenses/by-nc-nd/4.0/).

1. Introduction

Elucidation of the mechanisms and pathways of sediment transfer in glacial systems is necessary because the efficacy of basal sediment transfer modulates rates of subglacial erosion and patterns of landscape evolution (e.g. Alley et al., 2003; Swift, 2011; Egholm et al., 2012; Cook and Swift, 2012). In addition, glacial sedimentary deposits are key to understanding ice dynamics and thermal regime (and hence palaeoclimate) in Quaternary and ancient glacial systems (e.g. Evans, 2003; Hambrey and Glasser, 2012). Challengingly, transfer within glacial systems occurs via a complex and varied array of pathways reflecting different entrainment sources and processes. These pathways may include basal transport within till (e.g. Alley et al., 1997) or basal ice layers (e.g. Lawson, 1979; Hubbard and Sharp, 1993; Sharp et al., 1994; Knight, 1994; Knight et al., 1994; Sugden et al., 1987) and in englacial debris bands (e.g. Knight, 1987, 1994; Hubbard et al., 2004; Swift et al., 2006). The number and type of active pathways influences the overall capacity of sediment transport within the system, the volume and nature of material in transport, and the

* Corresponding author.
E-mail address: d.a.swift@sheffield.ac.uk (D.A. Swift).

character of deposits and landforms.

The terminal zones (i.e. snout areas) of many temperate, non-surging glacier systems in southeast Iceland, notably Svína-fellsjökull and Kvíárjökull, exhibit locally high supraglacial debris loads, exposures of debris-rich englacial and basal ice, and extensive arcuate frontal moraine systems. Supraglacial and proglacial debris characteristics at these glaciers is indicative of mixed transport from diverse (including fluvial and subglacial) pathways (e.g. Spedding and Evans, 2002; Swift et al., 2006; Bennett and Evans, 2012; Lukas et al., 2013). Debris emergence has been observed to occur via the melt-out of thrusts (Swift et al., 2006), 'channel fills' (i.e. englacial eskers) (Spedding and Evans, 2002), and debris-rich basal ice (Cook et al., 2007, 2010, 2011a). The abundance of fluvial material in glacial transport has been attributed to deposition of fluvial bedload within terminal overdeepenings (Spedding and Evans, 2002; Swift et al., 2006), whilst extensive exposures of debris-rich basal ice have been attributed to freeze-on of sediment-rich subglacial water as it ascends the adverse slopes of overdeepenings (Cook et al., 2007, 2010; Larson et al., 2010).

Terminal depositional materials and processes are strongly influenced by glacier structure (e.g. Evans, 2009; Bennett and Evans, 2012) and the distribution and volume of different basal ice types (e.g. Cook et al., 2011b). However, our understanding of the processes of debris entrainment by glacier ice and the development of debris-bearing ice facies and structures remains far from complete. Notably, the scope of many studies has been limited to the study of particular entrainment or transfer processes in isolation from their wider glaciological context, and from other processes within the same glacial system that may be spatially or genetically related. Further, it is rarely possible to observe entrainment processes at first-hand, meaning interpretation of the origin of englacial and basal facies and structures relies on inference from largely descriptive analyses using process-identification criteria that remain subject to debate (cf. Hubbard et al., 2009; Moore et al., 2010).

It is within the above context that we present evidence for complex, geomorphologically important terminal zone sediment transfer pathways at Svínafellsjökull in Iceland (Fig. 1). We describe transverse englacial debris-rich bands (Fig. 2) that contribute substantially to sediment transfer at the terminus, supplementing transfer in thick sequences of debris-rich stratified and dispersed facies basal ice (cf. Cook et al., 2007, 2010, 2011a). We present new physical analyses of debris band and basal ice exposures and sediments that provide novel insight into the geography and environments of their formation. From our observations, we propose that the overdeepened bed, which produces high longitudinal deviatoric stress and limits subglacial drainage system efficiency, results in transfer of locally high volumes of basal material of fluvial and subglacial origin in (1) englacial thrusts and (2) varied basal ice facies that reflect the hydraulic connectivity of the bed.

2. Field site and background

Svínafellsjökull (Fig. 1) is a temperate valley glacier that descends via a prominent icefall from the Öræfajökull icecap. Below the icefall, the tongue occupies an overdeepened basin situated behind an arcuate frontal moraine system (Fig. 1a, c), and well-developed band-type ogives are the dominant glacier structure. The terminus position has demonstrated little change since 1945 (Fig. 1c) and is presently situated on the adverse slope of a large frontal moraine system, where it upholds a series of minor ice-contact lakes (Fig. 1a). The subglacial topography of Svína-fellsjökull (Fig. 1c) has been derived from limited point survey radar survey undertaken in 1998–2006 (Magnússon et al., 2012).

Stratified debris-rich basal ice and anchor-ice terraces have been observed at many glaciers in southeast Iceland (Swift et al., 2006; Cook et al., 2007, 2010; Larson et al., 2010), all of which terminate on adverse slopes. Anchor-ice and stratified basal ice have physical characteristics similar to those at Matanuska Glacier, Alaska, that arise from glaciohydraulic supercooling of subglacial waters (Lawson et al., 1998). Larson et al. (2010) found that stratified basal ice samples from eight glaciers in southeast Iceland, including Svínafellsjökull (their Fig. 5F), contained thermonuclear-derived radioactive ^{3}H and was enriched in heavier isotopes (in δ^{18}O by ~2.4‰ and in δD by ~12‰) relative to subglacial water emerging from vents. These observations indicated that stratified ice was younger than the englacial ice and was consistent with open-system freezing of supercooled subglacial waters (cf. Alley et al., 1998; Creyts and Clarke, 2010). Cook et al. (2007, 2010), however, identified five distinct subfacies of stratified basal ice Svína-fellsjökull, only two of which were found to be consistent with supercooling. These two accounted for 42% of the stratified facies exposed at Svínafellsjökull and an estimated 83% of the stratified facies debris flux.

Englacial debris bands and dispersed facies basal ice have also been observed in southeast Iceland (e.g. Swift et al., 2006; Evans, 2009; Cook et al., 2011a). At Kvíárjökull, ~8 km to the southeast of Svínafellsjökull, Swift et al. (2006) observed that isotopic and sedimentary characteristics of debris bands were consistent with the thrusting of stratified basal ice to the glacier surface. Drawing on previous research showing that ogive formation is associated with transfer of basal material to the glacier surface along folds or thrusts (e.g. King and Ives, 1956; Goodsell et al., 2002; Swift et al., 2006; Cook et al., 2011a), Swift et al. (2006) concluded that band-type ogives had been reactivated by longitudinally compressive flow (cf. Moore et al., 2010) created by the adverse slope of Kvíárjökull's terminal overdeepening. Cook et al. (2011a) subsequently proposed that dispersed facies ice at Svínafellsjökull originated from strain-induced deformation and mixing of englacial (i.e. meteoric) ice with ogive-origin debris-band ice during travel in the basal zone of the glacier.

Work at Kvíárjökull indicates that deposition of material out of fluvial transport as channels enter overdeepenings could contribute significantly to the englacial and supraglacial debris loads of glaciers in the region. Spedding and Evans (2002) observed the melt-out of fluvial debris from channel-fills (i.e. englacial eskers) that indicated the presence of overdeepening-spanning englacial conduits. These have subsequently been documented by Bennett and Evans (2012) and Phillips et al. (2017). Swift et al. (2006) further observed the melt out of mixed subglacial and fluvial debris from englacial debris bands, implying thrusts were entraining fluvial materials deposited at the glacier bed. Our observations at Svínafellsjökull indicate similar complexity of sediment sourcing and a similarly large subglacial-to-supraglacial sediment flux in the terminus zone (e.g. Fig. 2).

3. Methods

Fieldwork was conducted in August 2005 and 2007 and in April 2015. Debris-bearing ice sequences and structures were observed and sampled at the glacier margin (where unobstructed by frontal lakes) and along three longitudinal (i.e. flow-parallel) transects (positioned where margin and glacier surface accessibility permitted) (Fig. 1a). Extensive crevassing of the terminus provided near-vertical, approximately flow-parallel views of englacial and basal ice structure. Basal and englacial ice facies and structures were characterised following Lawson (1979), including thickness, mean crystal diameter, debris distribution and concentration, and appearance, including the nature of internal layering and debris disposition (cf. Cook et al., 2011a). Structural information, including
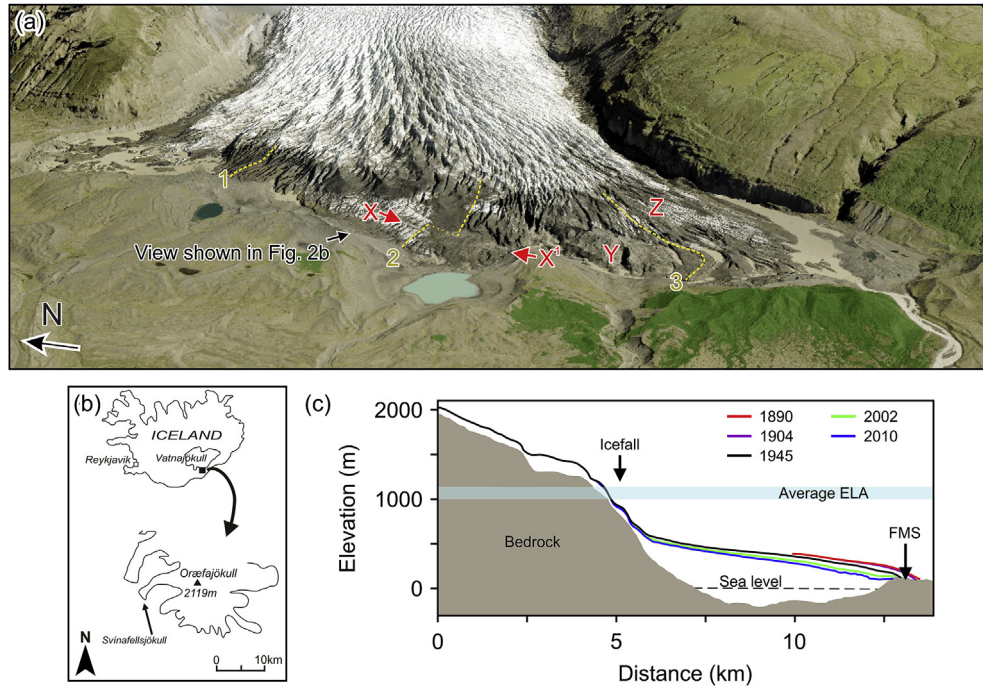
Fig. 1. (a): Oblique view of the terminus from LiDAR and aerial photography obtained in 2009. X and X¹ indicate the location of a prominent transverse supraglacial moraine shown in Fig. 2b. Y and Z are other prominent spreads of large calibre supraglacial debris. 1 to 3 indicates the locations of three structural surveys (see section 4.2). (b): General location of Svínafellsjökull. (c): Longitudinal profiles of Svínafellsjökull between 1890 and 2010 and average ELA determined from snowline altitude in MODIS imagery (redrawn from Hannesdóttir et al., 2015). FMS = frontal moraine system.
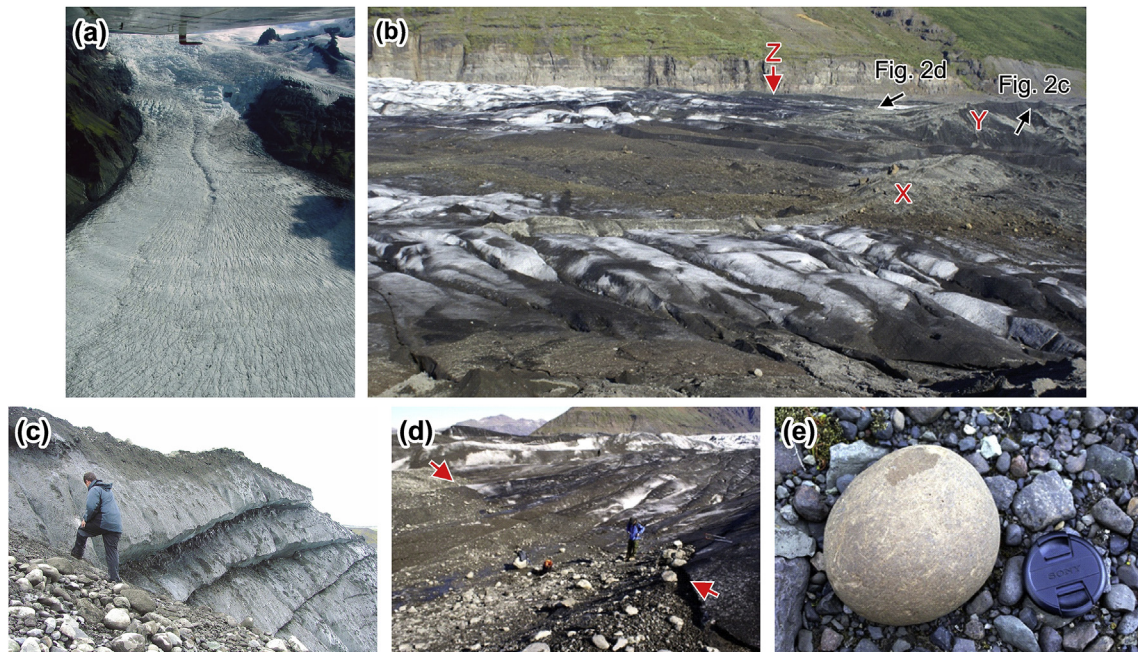

Fig. 2. (a): View of the icefall and upper tongue. (b): View over the central area of the terminus (see Fig. 1(a)). Ice flow is towards lower right. Darker areas of ice have superficial cover from melt-out of dispersed englacial ash and tephra deposits. Medium-toned areas reflect thicker debris cover, comprising clasts of variable size and morphology, including material indicative of fluvial, subglacial and supraglacial transport. Light-toned debris regions include conspicuous transverse ridges or localised accumulations of thick debris (X, Y, Z) with a large proportion of large-calibre rounded and well-rounded (RWR) clasts that are commonly striated. (c) and (d): Debris bands emergent within and upglacier of debris accumulation Y (see (b)). Arrows in (d) indicate the debris band location. (e): A well-rounded clast, photographed in the proglacial area, exhibiting striae and a percussion fracture, and therefore definitive evidence of post-fluvial active glacial (i.e. subglacial) transport.

the dip angle and direction of basal ice layers and englacial structures was also documented, and supplemented by structural mapping of the lower tongue from a orthorectified 2007 aerial image obtained by the UK's Natural Environment Research Council Airborne Research and Survey Facility (NERC ARSF). Detailed reviews of basal ice characteristics and classification schemes have been published by Hubbard and Sharp (1989), Knight (1997) and Hubbard et al. (2009).

Samples for stable isotope analysis (δ^{18}O and δD) were collected after removing 15−20 cm of surface ice to avoid surface water contamination (cf. Toubes-Rodrigo et al., 2016). The samples were then filtered within 24 h of collection through 47 μm cellulose nitrate filter papers and bottled in 8 ml Nalgene containers prior to analysis at the Scottish Universities Environmental Research Centre, East Kilbride, UK. Sediment retained during filtering was weighed to determine debris volume within each sample and further processed to determine the distribution of debris size. Material ≤ 1 mm diameter was analysed using a Coulter LS230 laser granulometer, with larger debris measured by sieve. X-Ray Fluorescence (XRF) analysis of basal ice debris was performed *in situ* in the field in April 2015 to further assess debris-band and basal ice provenance. A minimum of three XRF measurements per sample were performed using an Olympus DELTA Professional XRF device (60 s per measurement, 30 s per beam), again following the removal of the top 15−20 cm of ice to avoid surface contamination (Toubes-Rodrigo et al., 2016).

Large debris fractions were characterised in the field by analysis of clast shape (cf. Benn, 2004) and roundness (Powers, 1953) of typically 50 + basalt clasts (some samples were later combined). The same basalt lithology was sampled at each site to avoid uncertainties introduced by source lithology (cf. Lukas et al., 2013) and

because conglomerates are known to exist within the catchment that contain rounded non-basalt clasts. Presence or absence of striae on all clasts was recorded and values of relative angularity (RA, i.e. the proportion of angular and very angular clasts) and C_{40} (proportion of clasts with a c:a axial ratio of ≤0.4) were calculated (cf. Benn, 2004). For supraglacial debris spreads and in the proglacial area, the abundance of RWR clasts was further assessed by counting the total number exposed on the ground surface within a 25 m^2 area. Clast fabric analyses, which were limited by accessibility and number of clasts, were undertaken at two debris band and, for reference, two frozen subglacial diamicton exposures. This technique is used widely to interpret the transport or deposition history of glacigenic diamictons (i.e. clastic, matrix-supported deformable materials, including tills and basal ice) (e.g. Bennett et al., 1999; Benn, 2004). Clast fabrics within debris bands were measured by excavating through englacial ice above each band to expose the clasts within. Diamicton fabrics were measured by excavation of clasts from the exposure face.

No displacement was evident along debris bands during individual periods of field work. Glacier surface elevation change between 2007 and 2009 was therefore investigated instead, using aerial photographs and LiDAR collected by NERC ARSF. A 1 m resolution DEM for 2007 was produced from 30 cm resolution aerial photographs using Structure from Motion photogrammetry. The 2007 DEM was then subtracted from the 1 m LiDAR DEM generated from data collected in 2009 to yield an elevation change map (cropped to the 2007 glacier outline). Ground control was obtained by matching points with locations where no change was assumed to have taken place.
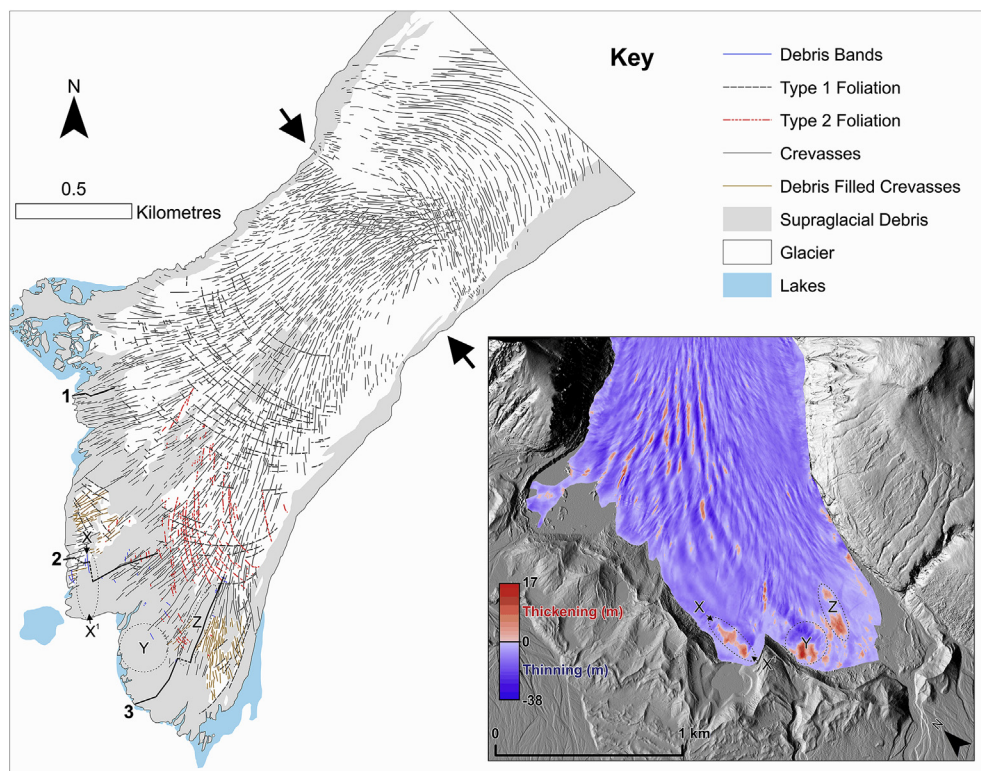

Fig. 3. Structural map of the lower tongue of Svínafellsjökull. 1 to 3 mark the positions of the flow-parallel surveys shown in Fig. 1a. X−X[1], Y and Z denote major surface debris spreads shown in Figs. 1a and 2a. Inset: Surface elevation change between 2007 and 2009 overlain on the 2009 LiDAR DEM hillshade. Areas of pronounced thickening (shown by red colouring) occur in the region of debris spreads X−X[1], Y and Z. Other areas of thickening relate to antiphase crevasse and serac migration between the datasets, rather than *in situ* surface changes. (For interpretation of the references to colour in this figure legend, the reader is referred to the web version of this article.)

4. Results

4.1. Structural context

Glacier surface structures in the lower c. 3.5 km of the tongue, including the terminus, are shown in Fig. 3. An arcuate, transverse crevasse field is present between 2.5 and 3.5 km from the terminus (upglacier of the two arrows in Fig. 3). Downglacier of this feature, these transverse crevasses close-up and are replaced by radial, approximately flow-parallel crevassing that extends to the terminus (a glacier planform known as a pecten). The cross-glacier ogive banding seen in Fig. 2a was not clearly apparent in this region, though two foliation types were observed: Type 1 being a relatively distinct but intermittent cross-glacier arcuate foliation; and Type 2 being a less distinct arcuate transverse foliation apparent only in the centre and true left of the lower 0.5–1 km of the glacier terminus. Debris bands were observed mainly in the central and southern region, within c. 100–600 m of the terminus. Localised areas of thickening were observed in the same central and southern region (Fig. 3, inset), specifically where surface debris accumulations were also present.

4.2. Basal and englacial structures and ice facies

4.2.1. General observations

Observed basal and englacial ice characteristics are summarised in Table 1. Basal ice stratigraphy was observed to conform to the generalized stratigraphy proposed by Knight (1994), which comprises a lowermost, debris-rich, layered facies, termed 'stratified facies', overlain unconformably by dispersed facies ice (cf. Cook et al., 2011a). The latter was in turn overlain by englacial (i.e.

meteorically derived) glacier ice, apparently conformably. The basal facies contained brown-grey sediment similar to that within subglacial diamicton though upper layers of dispersed ice (lower layers of englacial ice) sometimes contained more colourful tephra material. Englacial ice contained occasional debris bands consisting of a debris-rich stratified facies similar in appearance to that found in the basal ice layer. Stratified basal ice and debris band ice both contained layers of 'clean' (i.e. debris-free) ice between more debris-rich laminae (cf. Hubbard and Sharp, 1993; Hubbard et al., 2009).

4.2.2. Longitudinal survey 1

Extensive crevassing in the northern region of the terminus (Figs. 1a and 4a) permitted a limited (c. 250 m) survey of the glacier surface (Fig. 4b). Foliation on the survey demonstrated a general upglacier dip of 18° (Fig. 4b–d) and englacial samples obtained for isotope analysis (samples A to G) contained dispersed tephra (Table 1). Larger angular tephra clasts were present at the surface, as were a small number of well-rounded basalt clasts. Views left-and-right from the survey line (Fig. 4c and d) showed foliation-parallel banding of several m to 10s of metres thickness. A more steeply inclined, debris-containing fracture c. 75 m upglacier from the terminus (Fig. 4e) contained only tephra.

A c. 18 m long basal ice exposure below survey A-A' (Fig. 5a) comprised stratified and dispersed ice (Table 1) underlain by a frozen, well-consolidated subglacial diamicton. The diamicton was exposed manually by removing up to 0.5 m of adjacent water-logged and unconsolidated melt-out material. Three significant new features (cf. Cook et al., 2010) of stratified facies ice were observed:

Table 1
Characteristics and distribution of observed ice facies at Svínafellsjökull.

Facies	Survey 1	Survey 2	Survey 3	Facies code[a]
Englacial	Large crystal (mean 3.8 cm diameter) bubble-rich ice containing dispersed debris and <0.1% debris by volume[b] (volume insufficient for particle size analysis). Pervasive upglacier dipping transverse foliation. Healed crevasse structures dipped more steeply than foliation and contained little or no debris. Some angular aggregates and clasts up to 3 mm diameter of non-basal origin (survey 1).			N/A
Dispersed	Large crystal (mean 2.9 cm diameter) ice containing dispersed debris (<0.1 to 3% by volume[b]; mean 0.8 ± 1.3%; n = 7) comprising isolated particles and aggregates of silt to medium or coarse sand of 3 to 7 mm diameter. Generally massive and structureless though with occasional debris-rich planes (see Cook et al. 2011a). Isolated sub-angular and faceted sub-cm to cm diameter clasts of apparently basal origin.			SFB
Stratified	Medium crystal (0.5 to 3 cm diameter) ice, 0.1 to 3.2% debris by volume[c] (mean 1.0 ± 0.8%; n = 12), with mm-thick debris-rich and clean ice layers (though latter up to 3 cm thick). Debris layers comprise aggregates of silt/clay to granule gravel up to 4 mm diameter. Isolated faceted angular to rounded clasts up to 4 cm diameter.	Not present.	As survey 1.	SFA
Stratified-solid	Tight folds of cm to 10s cm thick bands of small crystal (sub-cm diameter) ice within stratified ice (above), 29.4 to 49.0% debris by volume[c] (mean 40.2 ± 10.3%; n = 4), with mm-thick debris-rich laminae comprising sand to granule gravel and sub-cm clean ice layers < 3 cm long. Faceted and striated clasts up to 4.5 cm diameter.	Not present.	As survey 1 but extensive up to metre thick exposures of gently rippled sub-horizontal mm to cm thick debris-rich and clean-ice laminae, poor sorting (debris-rich laminae comprised silt/clay to granule gravel), 37.3% debris by volume[c] (n = 1), numerous sub-rounded to rounded clasts, some up to 25 cm diameter, sparse angular clasts. Occasional cm-scale displacement of laminae on upglacier dipping shear planes.	SFD
Crevasse fill	Not present.	Diffusely laminated, small crystal (sub-cm diameter) ice, 0.3 to 2.7% debris by volume[c] (mean 1.3 ± 1.1%; n = 4), in narrow intensely deformed or sheared bands within dispersed ice (above), with texture qualitatively similar to nearby 'herringbone' crevasse-fill ice, 3.2 to 7.9% debris by volume[c] (n = 2) (see text).	As above but sub-vertical laminae with bifurcating structure, weak sorting but mainly sand to granule gravel, 22.4 to 25.0% debris by volume[c] (n = 2), no clasts and no apparent displacement of laminae along shear planes. Also 'herringbone' ice, 13.2 to 22.8% debris by volume[c] (n = 2), with intricate branching laminae structures of silt and fine sand.	N/A

[a] Code indicates equivalent facies type identified by Cook et al., (2010).
[b,c] Volumes determined by gravimetric analysis (see text); [b] Cook et al., 2011a; [c] this study.
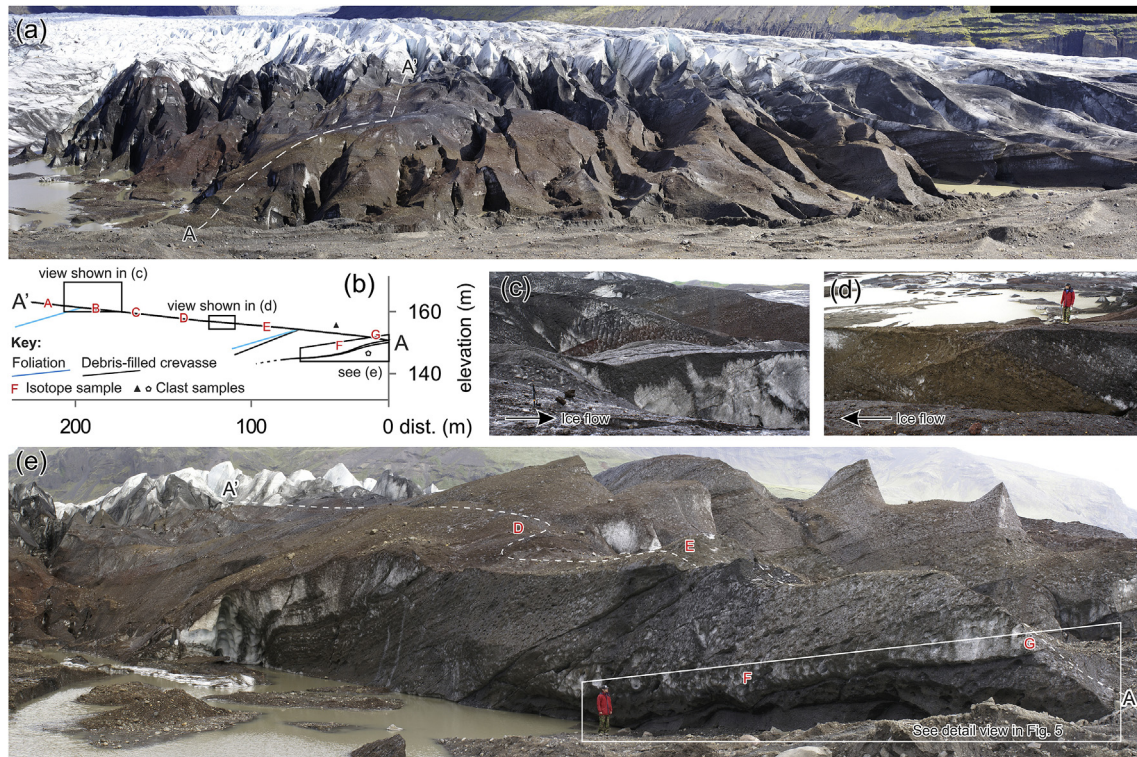
Fig. 4. (a): View of the northern area of the glacier terminus (ice flow is towards the viewer). Line of survey is indicated A–A'. (b): Survey line elevation and isotope sampling locations (letters); the location and dip of prominent foliation (blue) and debris-containing features (black) is also shown. Clast sample symbols indicate supraglacial (▲) and diamicton (pentagon) samples (Fig. 15). (c), (d): Views from the survey line showing foliation-parallel bands of ice defined by the colour of englacial debris (mainly tephra). (e): Context of the basal ice section shown in Fig. 4. (For interpretation of the references to colour in this figure legend, the reader is referred to the web version of this article.)
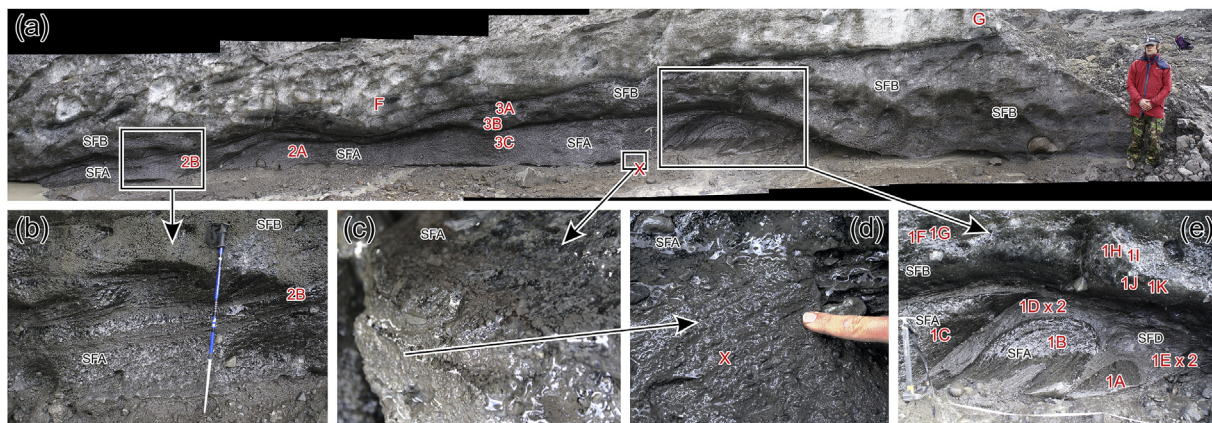

Fig. 5. (a): Detail of basal ice section in Fig. 4(e) showing facies types (black text; see Table 1) and isotope sample locations (red text). (b): Stratified facies exhibiting folding (tectonic thickening). (c), (d): Stratified facies situated above frozen subglacial diamicton, showing uniform upglacier dip of clean ice and debris-rich laminae both above and below the ice-diamicton boundary; X indicates the diamicton isotope sample location. (e): Several tight folds in stratified solid facies (SFD) ice containing stratified facies (SFA) ice (isotope sample locations are again indicated). (For interpretation of the references to colour in this figure legend, the reader is referred to the web version of this article.)

1. Debris laminae were observed to 'pinch together' to form 10 to 30 cm-wide bands. These exhibited higher debris concentration (c. 30–40% by volume) and a concomitantly higher concentration of clasts. Differential melt associated with the higher debris concentration had resulted in these bands forming prominent sub-horizontal steps (Fig. 5a).
2. Clean ice layers and debris laminations in stratified facies ice appeared to be contiguous with clean ice and debris layers within the frozen diamicton below (Fig. 5d). The debris laminae, comprising sub-centimetre debris aggregates and centimetre-

scale clasts (cf. Cook et al., 2010), appeared to originate from the solid debris layers in the diamicton (Fig. 5c).
3. Centimetre-scale clasts were occasionally observed at the point of being entrained from the clast-rich upper 'surface' of the diamicton. Several observations of this phenomenon were made at different locations in this region of the terminus.

4.2.3. Longitudinal survey 2
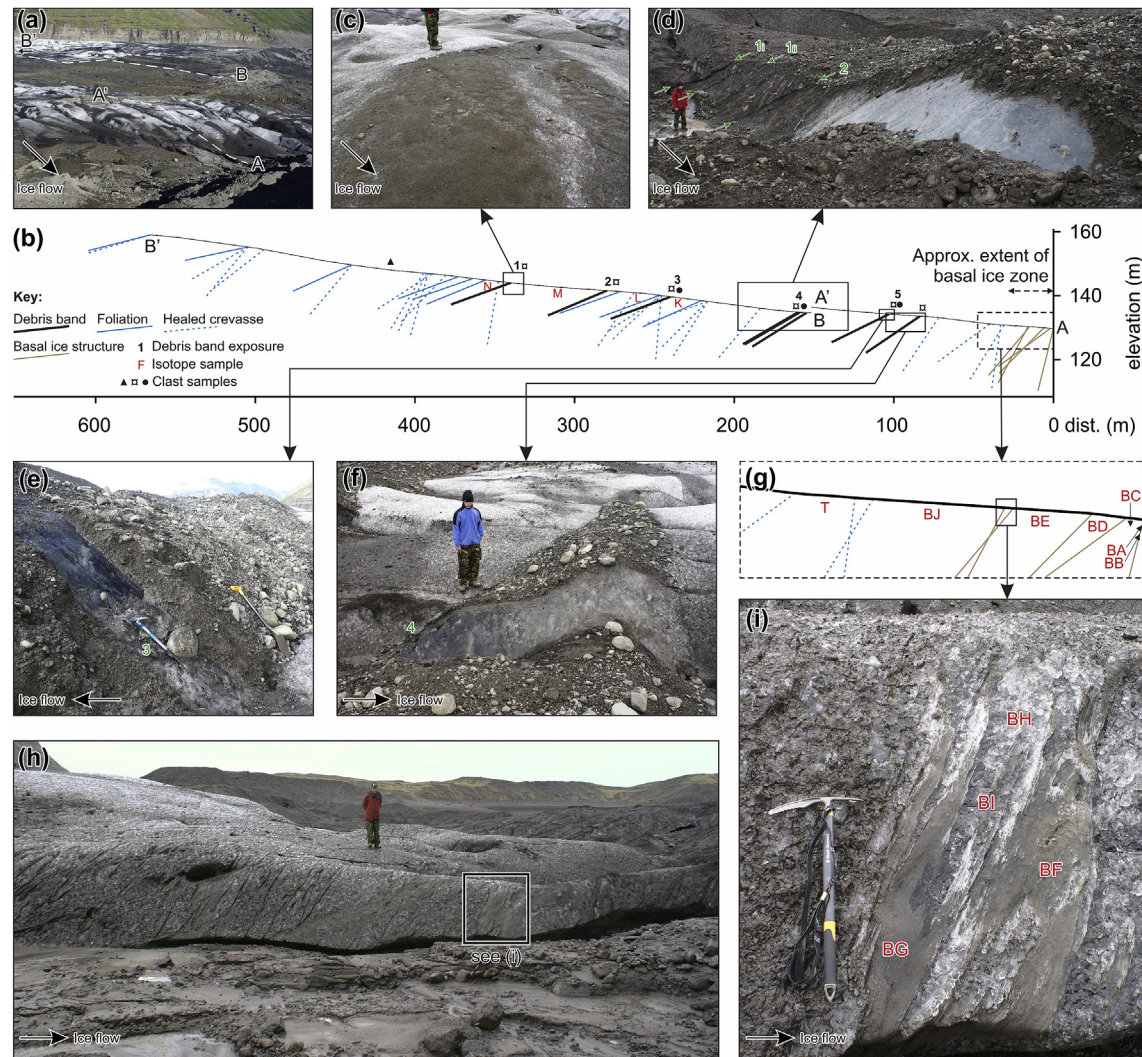Ice surface relief was generally low in the central region of the

Fig. 6. (a): View of central area of terminus showing survey 2. (b): Survey line elevation and key structures (see key). Isotope sampling locations indicated by coloured lettering. Clast sample symbols indicate supraglacial (▲), debris band (¤) and band-origin supraglacial debris (●) (see Fig. 15). (c) to (f): Examples of debris bands observed along the survey. A structural log (Fig. 10) encompassing bands 1 and 2 (see d) at exposure 4 and 3 and 4 (see e and f) at exposure 5 is described in the text. (g, h, i): Detail of basal ice section, also showing further isotope sampling locations.

terminus (Fig. 1a) and a c. 550 m survey (A-A′, B-B′; Fig. 6a) was undertaken from the terminus to the farthest up-glacier extent of visible surface debris. The survey line was offset laterally by c. 50 m at c. 150 m from the terminus to follow crevasses that afforded the clearest views of basal ice and englacial structures.

At the upper limit of the survey, foliation dipped upglacier at 12−14°. This dip steepened to 19−24° towards the survey midpoint (c. 350 m). Surface debris up-glacier of c. 350 m was a diffuse spread of fine-grained dark-coloured tephra in diffuse, ogive-like bands. The first debris-band structure (Fig. 6b) was observed c. 350 m. Debris bands down-glacier of this point exhibited a green-brown to brown-grey debris with small clasts that was consistent with the appearance of subglacial diamicton (see survey 1). Debris band dip was generally consistent with that of the englacial foliation, and both debris bands and foliation structures nearer the terminus exhibited a further steepening of dip to 32−34° upglacier (only a general sense of foliation dip could be obtained due to extensive debris cover). Foliated ice between debris bands was large crystal, low debris englacial ice.

Characteristics of debris bands varied along the survey. Bands

up-glacier of c. 200 m occurred singularly, had lower debris concentrations than those downglacier of this point, and were thin and laterally discontinuous (Fig. 6b). Nearer the terminus, bands were laterally extensive, exhibited higher debris content, including thick sequences of debris-rich and debris-poor ice, and occurred in more complicated sequences (Fig. 6c, d, e). Notably, a 'pair' of bands was observed at both exposures 4 and 5 (see 4.2.5, below), with the down-glacier band at each exposure exhibiting slightly steeper dip than the up-glacier counterpart. All bands exhibited a high proportion of RWR clasts, which is characteristic of fluvial sediment transport, and RWR clasts also exhibited striations, indicative of active glacial transport (detailed clast characteristics are described later). Melt-out from these debris bands was observed to be responsible for wide spreads of clastic supraglacial material and transverse ridges of the same material of several tens of metres to hundreds of metres in length. Clasts up to 50 cm in diameter were observed to have melted out from the bands (Fig. 6c, d, e).

The c. 30 m nearest the terminus comprised dispersed facies ice (Table 1) and, intercalated within, bands of finely laminated, both debris-rich and debris-poor, ice (e.g. Fig. 6f and g). The intercalated
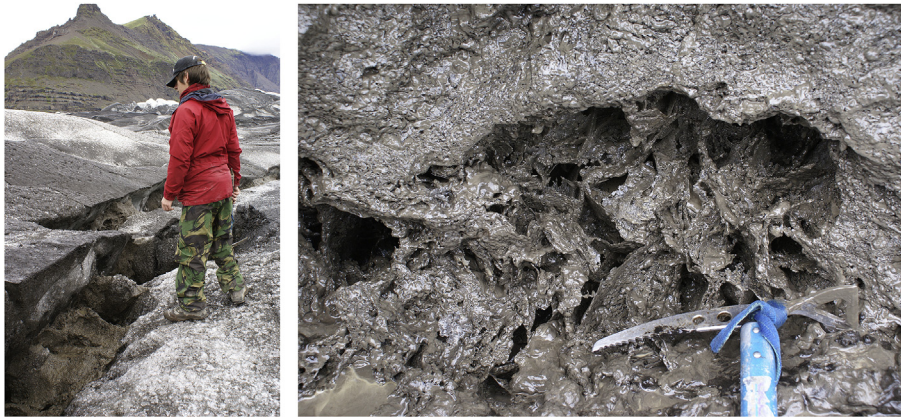
Fig. 7. Left: Crevasse fill near the ice margin, south of survey 2. Right: Close view of crevasse fill ice, showing platy and occasionally 'herringbone' structure and unimodal fine sediment distribution (cf. Fig. 13a) indicative of ice formation in gently upwelling glaciohydraulic supercooled water containing only fine suspended material (e.g. Cook et al., 2010, 2012).

ice exhibited lower sediment volume, smaller particle size and more diffuse lamination than stratified solid ice observed on survey 1, meaning it was qualitatively similar to nearby undeformed crevasse fill ice (Fig. 7). Stratified and stratified solid facies were not present. Melt out of basal layers precluded meaningful analysis of the relationship of basal ice to sediment below.

4.2.4. Longitudinal survey 3

The low-relief and partly flooded southern region of the glacier terminus comprises flow-parallel crevasse-defined ice ridges. A few exposures of basal ice were visible in 2005 in locations where ice ridges impinged on the proximal slope of the frontal moraine, but thinning and retreat meant that by 2007 the basal zone was mostly obscured by lake waters.

A c. 700 m survey (Figs. 1a and 8) extended to the farthest up-glacier occurrence of visible surface debris, where diffuse spreads of dark, fine-grained tephra coincided with the emergence of large-calibre, RWR material from several laterally discontinuous debris bands. These bands (Fig. 8c and d) were clast-rich but did not appear to contain debris-rich ice. Another set of bands emerged at c. 620 m (Fig. 8e) and a third single band emerged at c. 540 m (Fig. 8f). As observed on survey 2 (above), dip was generally consistent with englacial foliation, except for the uppermost set of bands, where foliation dip was more varied and steeper than observed elsewhere. Healed crevasses again exhibited steeper dip than surrounding foliation. The next set of bands occurred at c. 350 m, and, as on survey 2, were a pair of bands in which the lower band exhibited steeper dip (Fig. 8 g, h). Downglacier of c. 350 m, debris band exposures could not be observed closely due to limited accessibility caused by flooding of longitudinal crevasses, but these appeared consistent with exposures described above. All bands upglacier of c. 300 m were separated by large crystal englacial ice.

The sediment character and content of samples A to F (Fig. 8b) indicated that the final c. 120 m of survey comprised dispersed facies ice, with isotope samples G and F located just up-glacier from the start of the basal ice zone. An unusual vertical section at the end of the survey revealed >6 m of dispersed ice below a debris-rich structure or fracture of uncertain dip that may be a healed crevasse (as seen on survey 1). Many crevasse-fills containing vertically inclined layers of clean and debris-rich ice (e.g. Fig. 8j) were observed in this region. Vertical exposures of horizontally layered stratified solid ice were also observed, situated below stratified facies, in 2005 (Table 1, Fig. 9). In contrast to survey 1, the boundary between stratified and stratified solid ice was

unconformable, with laminae in stratified ice being more steeply inclined than the laminae in stratified solid ice below (Fig. 9).

4.2.5. Details of debris band character and context

Detailed logs were undertaken at exposures 4 and 5 (Fig. 6b) on survey 2, encompassing two band 'pairs' comprising bands 1 and 2 at exposure 4 (see Figs. 6d), 3 and 4 at exposure 5 (Fig. 6e and f, respectively). Logs were taken horizontally and key observations have been transposed onto a vertical scale representative of a vertical log through the ice (Fig. 10). At exposure 4, the up-glacier band comprised two apparently separate structures (1i and 1ii in Fig. 6d), separated by large-crystal englacial ice, with the lower band (1ii) containing clasts but no debris-rich ice. The down-glacier band at exposure 4 (2 in Fig. 6d) also comprised two obvious but more closely adjacent structures, with ice between the structures being 'cross-cut' by more steeply dipping debris septa with a sediment content and character similar to that within the 'main' bands. At exposure 5, the up-glacier band (3) and down-glacier band (4) were again separated by englacial ice. Isotope samples of band ice were obtained from the thicker bands to avoid contamination from adjacent englacial ice.

Bands exhibited high clast content and alternating centimetre-scale layers and lenses of both clean and debris-rich ice. Overall band thickness ranged from 5 to 25 cm and internal layers exhibited similar but sometimes slightly steeper dip to that of the 'parent' band. Debris laminations (particularly bands 2, 3 and 4) were similar to those in stratified facies basal ice (Table 1). Debris comprised a wide range of grain sizes, but mainly medium to coarse sand and granule gravel with a lesser component of silt and clay. 'Clean ice' lenses within band ice were typically 1.5−2 cm thick (occasionally up to 3 cm), contained isolated debris aggregates ~2−3 mm in diameter composed mainly of medium to coarse sand, and pinched out laterally over several cm or tens of cm. Debris-rich ice laminae were thinner, typically 1 cm or less. Clasts were strongly aligned with glacier flow direction (see later).

Two notable observations were made that have not previously been reported of englacial debris bands. First, the upper contact between band ice and glacier ice was typically sharp and marked by a clast-rich layer in which clasts were very strongly aligned with flow direction. Second, the boundary between band ice and the glacier ice below was indistinct and clast-poor, with trails or septa of finer debris that diverged from the main band into englacial ice below. These contained occasional clasts up to 1 cm diameter, again oriented in the direction of flow.
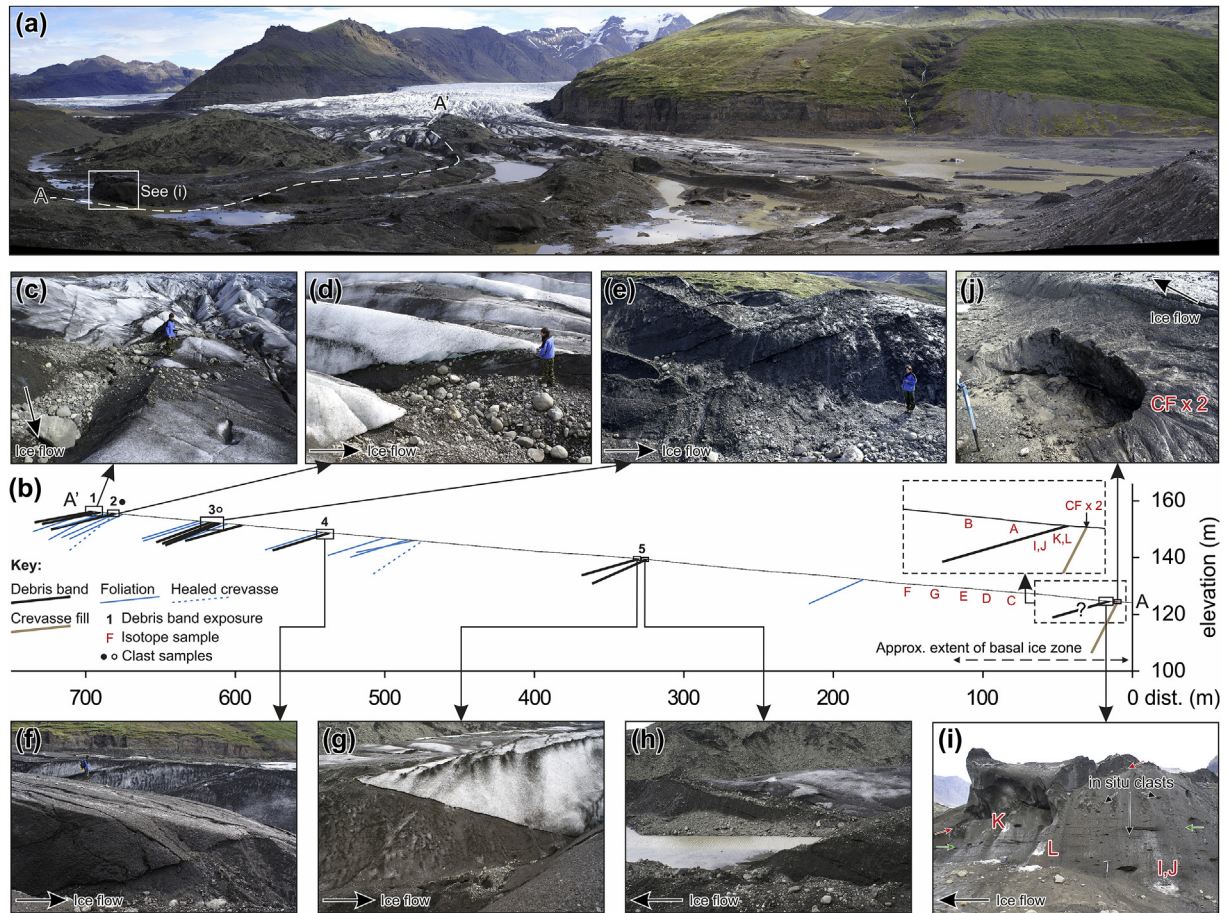
Fig. 8. (a): View of southern area of terminus showing survey 3. (b): Survey line elevation showing foliation (blue), healed crevasse (blue dashed) and debris band (black) exposures (numbered). Isotope sampling locations of firnified glacier ice and basal ice are labelled A to L. Clast sample symbols indicate band-origin supraglacial debris clast form sample (●) (see Fig. 15) and rounded clast count (○) (Fig. 18b) locations. (c) to (h): Debris band exposures. (i): Basal ice section near terminus, also showing isotope sampling locations I to L. Red arrows indicate possible thrust of uncertain dip; green arrows indicate quasi-horizontal layering in SFB. (j): Crevasse fill with vertically inclined layering, showing location of isotope sample H. (For interpretation of the references to colour in this figure legend, the reader is referred to the web version of this article.)
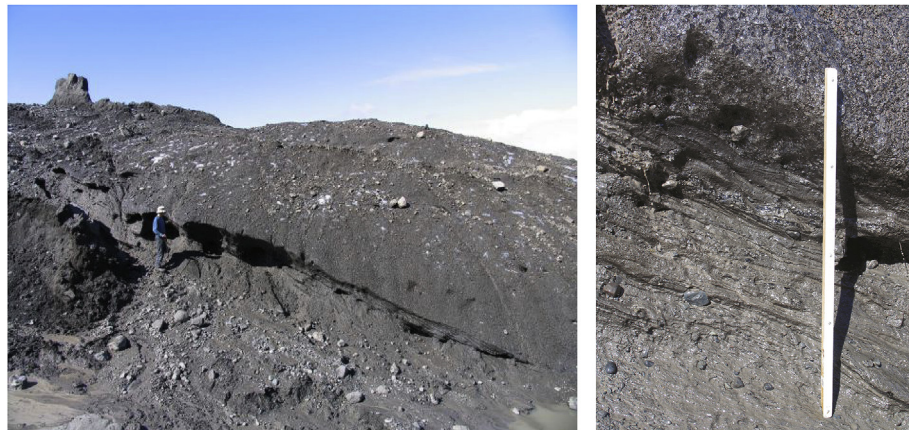

Fig. 9. Left: A basal ice exposure in the southern region of terminus, observed in 2005. Right: Detail of the same exposure with metre rule for scale, showing quasi-horizontally layered stratified solid ice with stratified ice resting unconformably above.
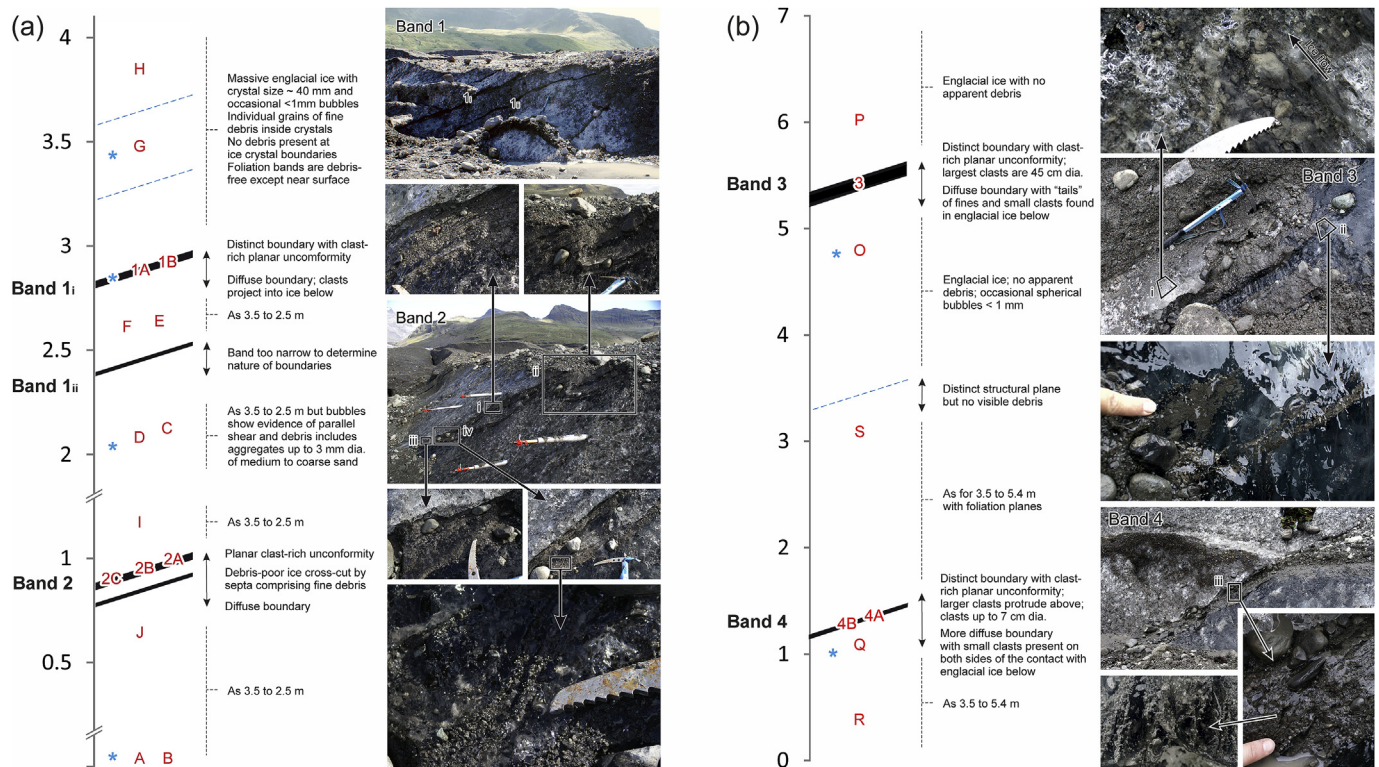
Fig. 10. Vertical logs through debris bands and adjacent ice at exposures 4 (a) and 5 (b) on survey 2. Y-axis values are in metres. (a) Log through bands 1 and 2 at exposure 4 (see Fig. 6d). Left: Sedimentary log, showing location of isotope (letters) and ice crystal samples (* symbols), and major ice facies and band characteristics. Note the breaks in y-axis values. Right: Photos include close-views of several band characteristics (ice axe for scale). i: Sharp upper boundary between band ice below and firnified glacier ice above; ii: Fold in band ice beneath the main 'active' band; iii: Larger clasts at upper band surface, demonstrating strong fabric in ice flow direction; iv: Close view of stratified ice layering crossing clean ice sandwiched between upper and lower band surfaces. Stakes shown in the central photo of Band 3 were monitored for c. 10 days during summer 2007, but no displacement was observed. (b) Log through exposure 5 encompassing two further bands (3 and 4; Fig. 6e and f, respectively). Left: Sedimentary log. Right: Photos include close-views of several band characteristics. i: Clast rich upper band surface viewed through firnified glacier ice; ii: Tails (or trails) of finer debris extending into firnified glacier ice below the band; iii: Clast-rich upper band surface and view of band ice sample obtained from below the upper band surface.

4.3. Physical characteristics of materials

4.3.1. Stable isotope characteristics

Stable isotope data (expressed as $\delta^{18}O$ and δD relative to V-SMOW) from samples collected from Svínafellsjökull in 2007 (Table 2) complement equivalent data reported in previous work by Cook et al. (2010, 2011a) and add substantially to the existing dataset. Isotope data pertaining to dispersed facies ice samples from 2007 has previously been discussed by Cook et al. (2011a).

Envelopes encompassing the full range of stable isotope data of each main facies type (with one exception; see below) are shown in Fig. 11a. The complete data (with the same envelopes) are plotted in Fig. 11b and e. Debris band ice was found to be isotopically heavier than englacial ice, with only slight overlap of their respective envelopes. Crevasse-fill ice samples were significantly heavier still, and had a very narrow composition envelope that was non-overlapping with englacial ice. Dispersed and stratified ice samples demonstrated large envelopes, with the dispersed envelope overlapping englacial ice and debris band envelopes, and the stratified envelope overlapping the dispersed, debris band and crevasse-fill ice envelopes. Compositionally, the subglacial diamicton sampled on survey 1 was isotopically heavier than the debris band ice and was situated in the zone of overlap between dispersed and stratified ice.

After exclusion of four stratified ice samples from survey 2 that were suspected to be deformed crevasse-fill ice (samples BA, BB, BF, BG), only two stratified samples obtained in 2007 overlapped with the crevasse fill envelope (stratified solid samples 1D and 1D2 on survey 1). Finally, one dispersed sample (BC on survey 2) fell significantly outside the envelope for dispersed samples, being situated instead within the debris band ice envelope.

Table 2
Summary of ice sample stable isotope compositions.

Sample	N	Mean $\delta^{18}O \pm \sigma$ ‰	Range $\delta^{18}O$ ‰	Mean $\delta D \pm \sigma$ ‰	Range δD ‰
Englacial ice	22	-12.3 ± 0.3	-12.6 to -12.0	-74 ± 2	-76 to -70
Debris band ice	8	-11.2 ± 0.8	-12.4 to -9.9	-69 ± 3	-72 to -65
Dispersed ice	15	-11.7 ± 1.4	-14.2 to -9.4	-75 ± 7	-88 to -60
Stratified ice	14	-10.9 ± 0.8	-12.5 to -10.0	-73 ± 4	-78 to -66
Stratified ice (solid)	4	-9.3 ± 0.9	-10.3 to -8.3	-61 ± 8	-68 to -53
Crevasse fill ice	4	-8.6 ± 0.3	-8.9 to -8.3	-53 ± 4	-58 to -47

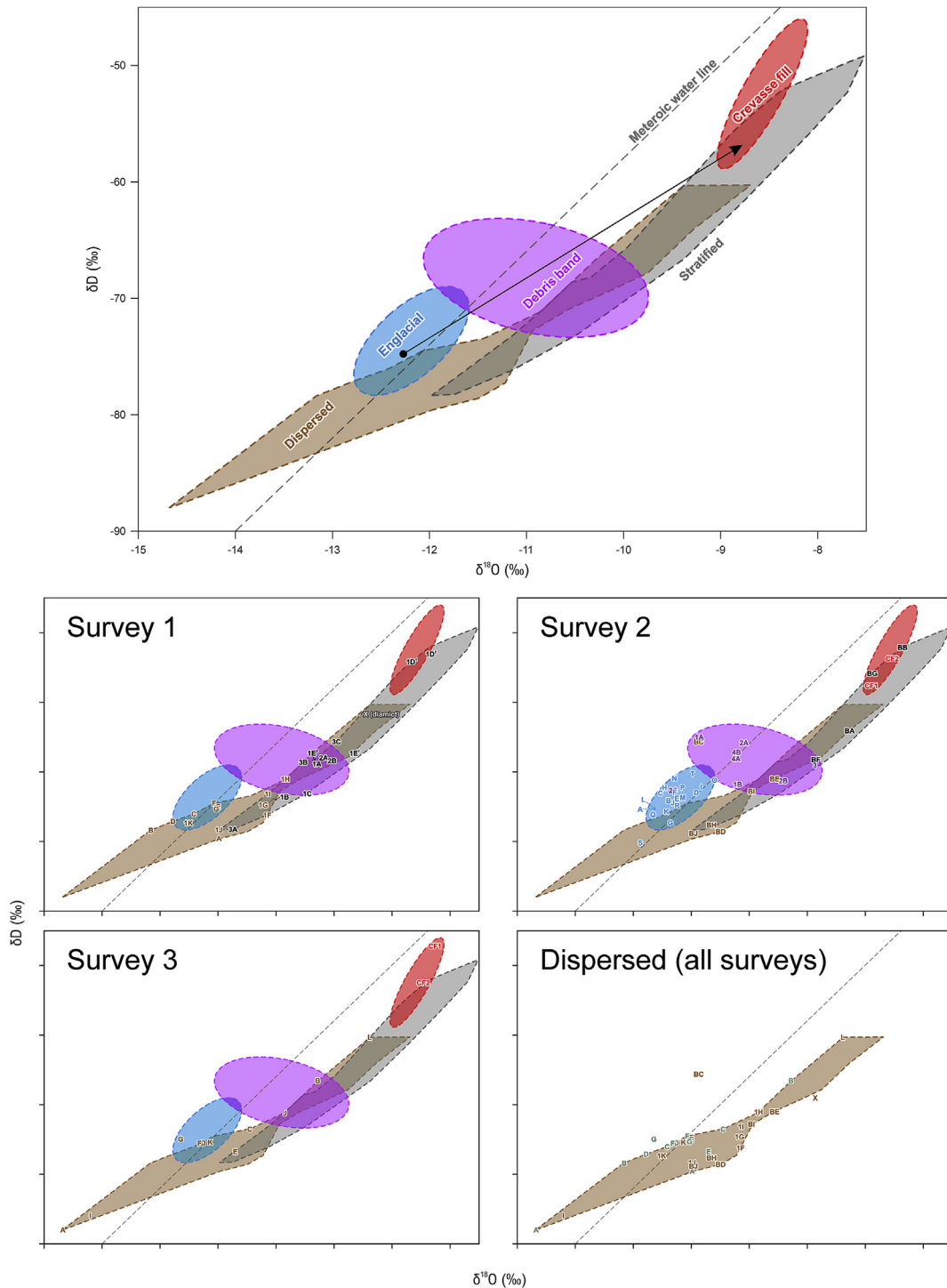**Fig. 11.** Isotopic composition (δ18O against δD) of debris band ice, firnified glacier ice and basal ice facies sampled in 2005 and 2007. Upper diagram summarises sample envelopes. The black arrow shows predicted offset in composition after open system refreezing of ice with an average firnified glacier ice composition (cf. Cook et al., 2010). Lower diagrams show compositions of samples on individual surveys. The meteoric water line has been adjusted to plot through the samples from Svínafellsjökull. Englacial samples containing dispersed tephra (see text) are included in the dispersed envelope in all diagrams and are shown plotted separately in green in the final panel. (For interpretation of the references to colour in this figure legend, the reader is referred to the web version of this article.)
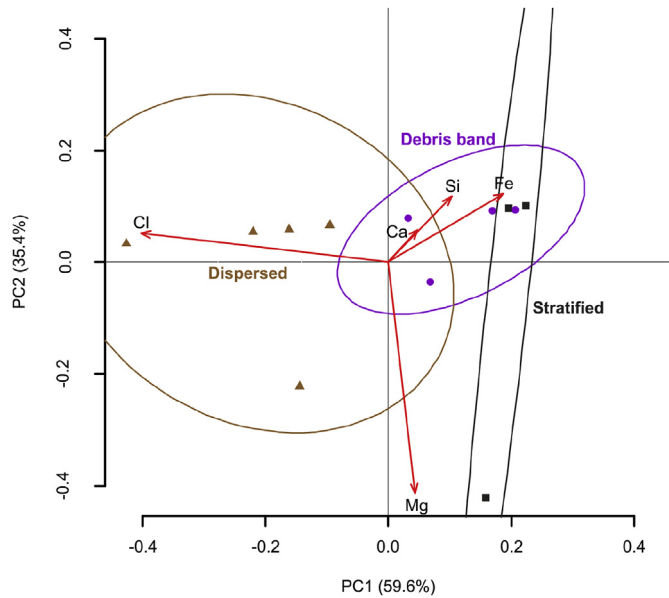
Fig. 12. Biplot showing results of Principal Component Analysis of XRF element data from 2015 basal ice and debris band samples. Envelopes are drawn for a confidence interval of 95%. Leading elements for the differences were chlorine (Cl), which was more abundant in dispersed facies ice, and iron (Fe) and silica (Si), which were more abundant in stratified ice.

4.3.2. XRF analysis of basal and debris band ice

Three ice types were analysed using XRF in 2015: dispersed facies basal ice; stratified basal ice; and debris-band ice. Principal Component Analysis (Fig. 12) of sample elemental composition data demonstrated that dispersed and stratified basal ice facies occupied distinct, non-overlapping populations. Debris band ice was, compositionally, situated between that of dispersed and stratified types, and partly overlapping with both.

4.3.3. Basal ice and debris band particle size distribution

Debris band mean sediment size distribution is presented in Fig. 13a alongside distributions for a range of basal ice facies samples (Cook, 2006) and several samples obtained in 2007 from frozen subglacial diamicton beneath basal ice layers at or near survey 1.
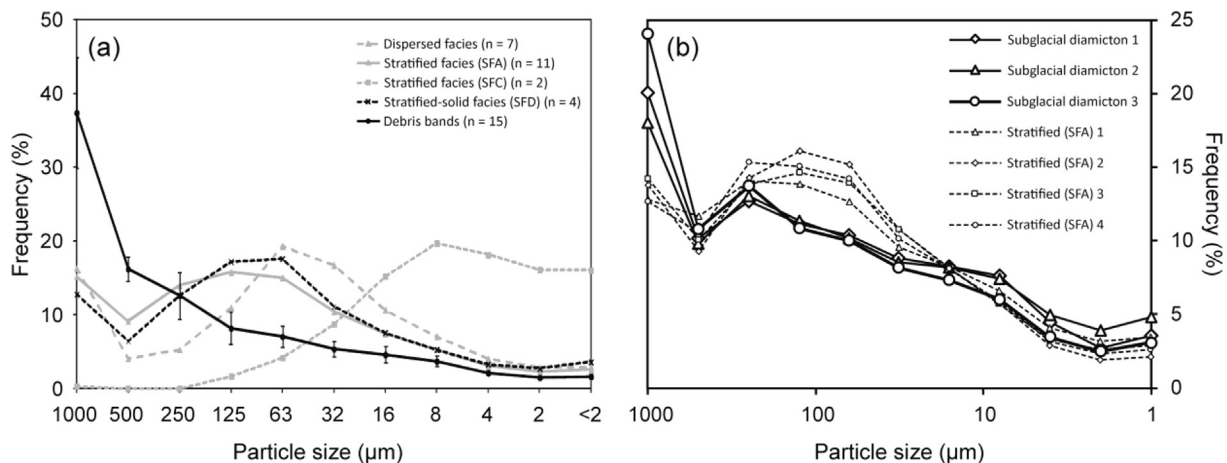
In general, crevasse-fill ice (cf. Fig. 7; SFC in Fig. 13a) demonstrated the finest sediment size distributions, with relatively little material >32 μm, followed by dispersed, then stratified solid ice, and stratified ice, which all exhibited a peak in size distribution between ~32 and 125 μm. Debris band materials were coarser still and exhibited a distribution distinct from other basal ice types due to having a greater coarse sand fraction (500–1000 μm) and relatively smaller volumes of finer size fractions. Debris band distributions were therefore closest to diamicton sample distributions (Fig. 13b), whilst basal ice distributions were dissimilar to those of diamictons sampled beneath. Notably, stratified facies samples demonstrated a reduced volume of material in the ~1000 μm and <32 μm fractions relative to diamicton samples (Fig. 13b), and, consequently, a relative enrichment in the ~32–125 μm fraction. Distributions shown by individual samples of stratified and diamicton, in contrast, show good consistency (Fig. 13b). Because laminae in the stratified facies ice observed at survey 1 was apparently contiguous with that in the diamicton beneath (e.g. Fig. 4c and d), these differences in size distribution may be pertinent to the process of stratified ice formation.

4.3.4. Clast fabric and form

Clast fabric samples from debris bands on survey 2 showed moderate to strong preferred clast orientation in the direction of ice flow (Fig. 14), with strong upglacier dip due to the c. 20° upglacier inclination of the bands. For subglacial diamicton samples, strong orientation in the direction of flow and upglacier dip was again observed, although a minority of clasts dipped downglacier, which is a commonly observed characteristic of subglacially deposited diamictons (Benn, 2004).

Clast form data (Figs. 15 and 16) show that scree and supraglacial debris samples were dominated by very angular clasts, had relative angularity (RA) values of 100%, displayed no signs of striation, and had high C_{40} values (64% and 27% respectively) that indicate a wide range of clast shapes including blocks, elongates and slabs. Analysis of data for other samples revealed that:

1. Supraglacial (centre) material was dominated by angular and sub-angular clasts, had a low C_{40} value indicative of predominantly blocky shapes, and 17% of clasts exhibited striations.

Fig. 13. Sediment particle size distributions for debris band, basal ice, and subglacial diamicton samples. (a) Distributions for basal ice (Cook, 2006; Cook et al., 2010) and debris band samples (this study). Dispersed facies and stratified facies A and D are described in Table 1. Stratified facies C (cf. Cook et al., 2010) were observed to connect with 'crevasse fill' features (cf. Fig. 7). (b) Distributions of stratified facies ice A and subglacial diamicton samples (this study).
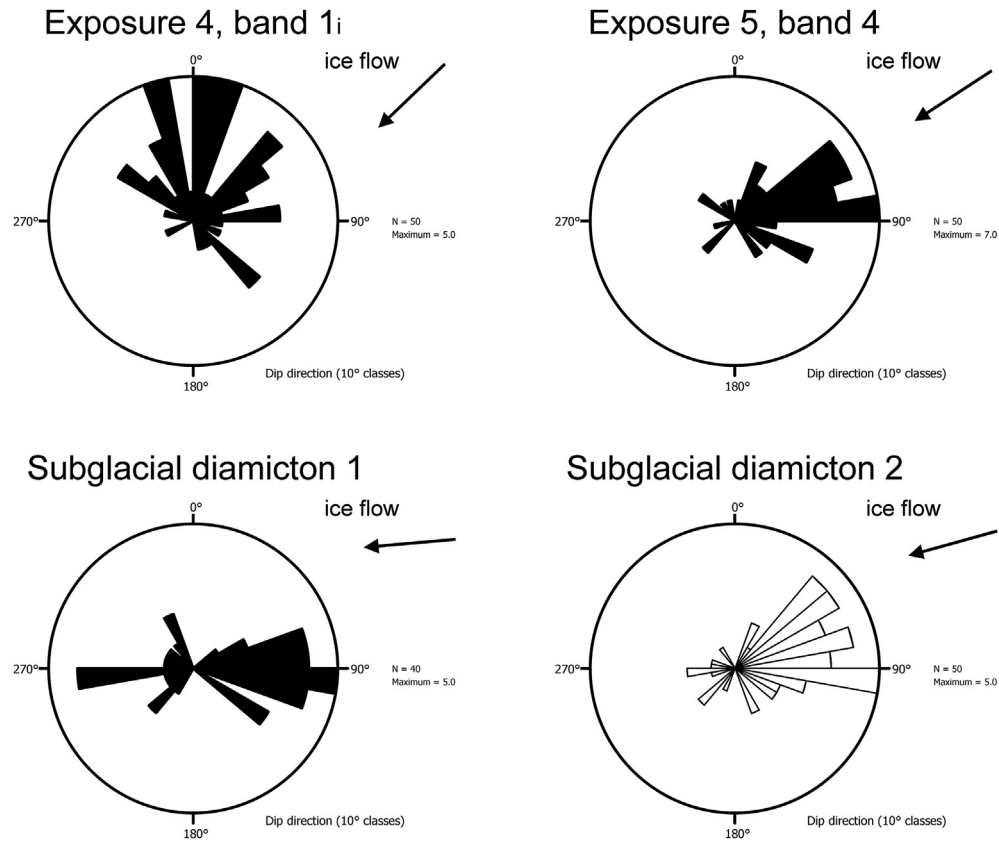
Fig. 14. Uni-directional rose diagrams showing clast orientation and dip for samples of clasts from two debris bands and two frozen subglacial diamicton units. The approximate direction of ice flow, determined by analysis of aerial photography, is shown for reference.

2. Samples from debris bands and their associated supraglacial moraines exhibited similar form characteristics to those of basal ice and subglacial diamicton samples, with distributions dominated by sub-angular clasts, few (or no) very-angular clasts, and relative angularity ranging from 6 to 49% (mean 22%), C_{40} values below 32% (mean of 16%), and striation incidence ranging from 15 to 90% (mean 40%). Of these, debris band samples exhibited the highest relative angularity (RA) and lowest relative roundness (RR), followed by associated moraines, and stratified solid ice and subglacial diamicton samples.

3. Debris band, stratified solid basal ice and diamicton samples typically included a notable proportion of rounded and well-rounded (hereafter RWR) clasts, with relative roundness values ranging between 3 and 8% (mean 5%) for debris bands and as high as 12 and 17% for basal ice and diamicton. All samples except one in this group (a subglacial diamicton sample) exhibited striations on between 50 and 100% of RWR clasts (mean 74%).

4. Excluding supraglacial materials, debris band samples exhibited the most variable RA and C_{40} values, with greatest variability occurring in the RA value. Notably, RA values were in general highest (>20%) for upglacier debris bands (notably, sites 1 to 3 on survey 2 (Fig. 15 h to j) and site 2 on survey 3 (Fig. 15j)) and lowest (<20%) for the lowermost debris bands (notably, sites 4 and site 5 band Y on survey 2 (Fig. 15d to g)).

5. Proglacial moraine sample RA, RR and % striated values were more similar to those of debris band and associated moraine samples than to subglacial diamicton samples, the latter having the highest proportions of striated clasts.

5. Discussion

5.1. Debris band origin

Debris bands are common across a range of glacier types (e.g. Swift et al., 2006; Hubbard et al., 2004; Larson et al., 2010; Lovell et al., 2015) and thrusting is accepted as the principal explanation for their formation (e.g. Evans, 2009). However, thrust mechanisms, identification criteria, and debris entrainment processes and sources remain much debated (e.g. Weertman, 1961; Hooke and Hudleston, 1978; Woodward et al., 2002, 2003; Glasser et al., 2003; Hambrey et al., 1996, 1997, 1999; Hubbard et al., 2004; Lukas, 2005; Graham et al., 2007; Moore et al., 2010).

Large longitudinal compressive strain rates associated with warm to cold-based ice transition zones of polythermal ice masses are most commonly invoked as explanations for thrusting, though Swift et al. (2006) concluded that suitably large compressive strain rates are also generated in temperate ice by the adverse slopes of overdeepenings. Nonetheless, the process likely requires thin ice or optimally oriented pre-existing fractures that are in hydraulic communication with high-pressure subglacial water (Moore et al., 2010), with suitable structures in temperate ice including those associated with band-ogive foliation (e.g. Swift et al., 2006). Further, thrust-like debris septa can be generated by alternative processes, including debris emplacement into thrusts or englacial crevasses by englacial conduits (cf. the conduit fills of Spedding and Evans, 2002) where subglacial channels meet overdeepenings (Fountain and Walder, 1998; Cook and Swift, 2012), or by injection of high-pressure turbid subglacial water into basal crevasses (e.g. Ensminger et al., 2001; Lovell et al., 2015).
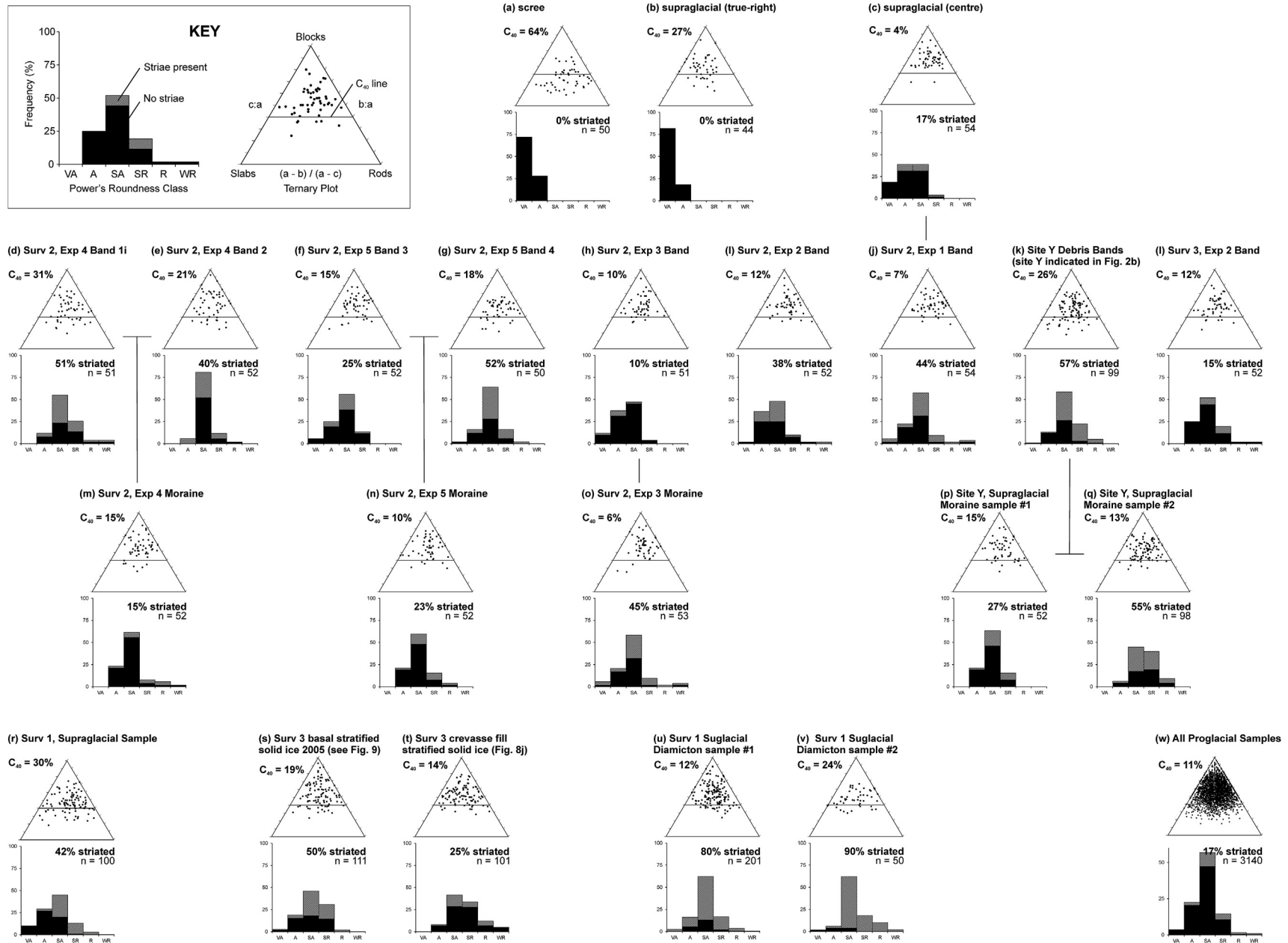
Fig. 15. Clast shape ternary diagrams and roundness histograms for samples of scree and supraglacial debris (row 1); debris bands (row 2); supraglacial moraines (row 3); and near-terminus supraglacial, basal ice, subglacial diamicton, and proglacial moraine complex samples (row 4). Connecting lines indicate up/downglacier associations between samples. Ternary diagrams are plotted with the c:a axial ratio on the left axis, b:a axial ratio on the right axis, and (a−b)/(a−c) on the horizontal axis. The horizontal line represents the c:a axial ratio of 0.4, known as the C_{40} value. Histograms are plotted with the Powers (1953) roundness scale on the x-axis and the frequency up to 100% on the y-axis. The proportion of striated clasts in each roundness category is shown (see key) and the overall proportion of striated clasts is given in %. Ternary diagrams have been plotted using the TRIPLOT program of Graham and Midgley (2000).
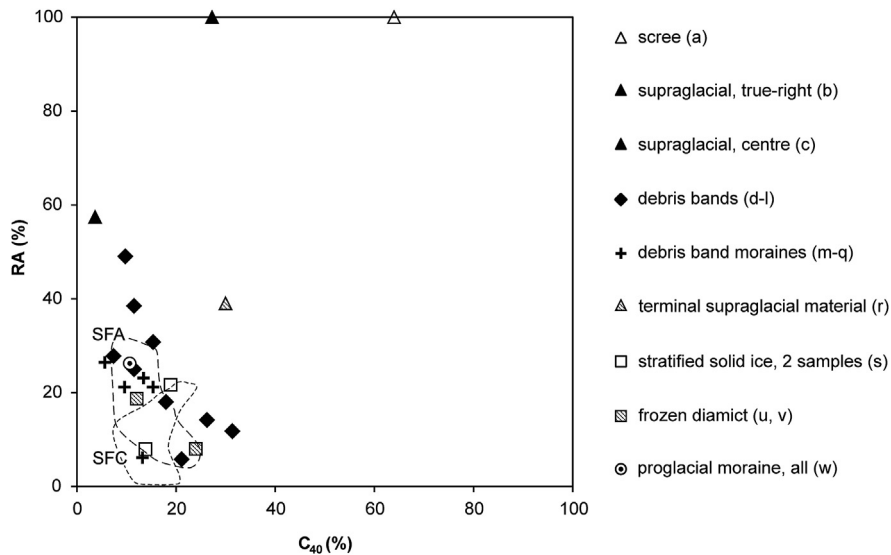
Fig. 16. Bivariate plot of C_{40} against Relative Angularity (RA) for clast samples shown in Fig. 15. The two stratified solid ice samples (shown combined in Fig. 15s) are plotted separately. Envelopes of stratified basal ice clast samples from Cook et al., (2011b) are shown (dashed lines) for comparison (stratified basal ice subfacies A is formed by regelation; subfacies C is formed by freeze-on of supercooled water as a consequence of glaciohydraulic supercooling).

5.1.1. Debris band character

At Svínafellsjökull, debris bands contain large-calibre debris with a notable incidence of RWR clasts, many of which are striated (e.g. Fig. 15, d to l). Debris band sediment calibre (i.e. size) and character was, however, variable, and bands in general were characterised by stratified facies ice with predominantly sub-angular clasts (Fig. 15). Band ice was therefore similar in physical appearance to that of stratified ice found within the basal ice layer (this study, but see also Cook et al., 2007, 2010) and inconsistent with freezing in situ (e.g. in water-filled crevasses; Ensminger et al., 2001; Roberts et al., 2002). We therefore argue that debris bands at Svínafellsjökull have been produced by thrusting.

Two observations of physical appearance particularly support thrusting. First, clast orientation within bands was strongly clustered and aligned with ice flow direction (cf. Lovell et al., 2015), in one case displaying fabric strength similar to that of subglacial diamicton (Fig. 14). Such clustering is characteristic of simple shear, which leads to clasts becoming oriented semi-parallel to the shear surface (e.g. Hicock, 1991). Second, crude upward coarsening and increasing incidence of clasts resulted in a clast-rich layer at the upper surface of each band (Fig. 10), which indicates a sorting process similar to that responsible for armoured substrate surfaces in fluvial and aeolian environments (e.g. Knighton, 1998) and 'boulder pavements' in deformation-dominated subglacial till or lodgement till (Hicock, 1991; Krüger, 1994). The absence of a distinct lower boundary to the bands, and the observation of 'trails' of fine sediment in apparently englacial ice below, implies simple shear is confined to the upper 'surface' of the band, with deformation below this surface leading to mixing of debris band ice and debris with firnified glacier ice below. Occasional irregularities in band thickness (e.g. Fig. 10 b and Fig. 3) may represent the incorporation of 'rafts' or blocks of material along the thrust.

Four further observations also provide support for thrusting. First, stable isotope data for debris band samples (Fig. 11; discussed below) demonstrate an unusual envelope that does not indicate a specific refreezing process (i.e. formation of ice from a single water source). Rather, the envelope partially overlaps with the envelopes for englacial, dispersed and stratified ice samples (Fig. 11), indicating strain-induced mixing of these ice types to various extents

(cf. Sharp et al., 1994; Hubbard et al., 2000; Cook et al., 2011a). Such mixing of ice from different sources is consistent with entrainment of materials from the glacier bed by a combination of simple-shear and strain-related deformation. Second, XRF results show that debris band ice is compositionally between that of dispersed facies and stratified facies basal ice (Fig. 12), which implies mixing by deformation of normally distinct basal ice layers prior to (or during) incorporation into the thrust.

Third, the high proportion of RWR clasts in debris band samples that were striated (Fig. 15) indicates a mixed transport history involving initially fluvial and then active subglacial transport. This could occur post-entrainment as a result of shearing along the bands; however, there is evidence of active subglacial transport prior to entrainment of clasts into bands due to the decreasing angularity of clasts within the debris bands with decreasing distance from the terminus (Fig. 15), which indicates a longer subglacial transport distance of clasts in downglacier bands. Finally, clast size observations and particle size data (Fig. 13) demonstrated that debris bands and debris band ice samples contained coarser sediment than other basal ice types, indicating entrainment from the basal layer of a wider range of material sizes than is typical of basal ice formation alone.

5.1.2. Structural context and sediment source

At Svínafellsjökull, two internal foliation types were visible, and debris band strike appears to be most closely aligned with that of the less distinct Type 2 foliation (Fig. 3). This relationship could not be confirmed in the field because observations of strike were limited by surface crevassing, short accessible band ice exposures, and the uneven surface. Nonetheless, along-flow exposures afforded by longitudinal crevasses demonstrated that debris band dip was generally consistent with visible internal foliation (see 4.2.2–4), whereas healed crevasses – the only other prominent internal structure – were notably steeper. Relatively distinct Type 1 foliation is therefore assumed to represent transverse crevasses traces that originate during extensional flow c. 2.5–3.5 km from the terminus (Fig. 3). Type 2 foliation is likely therefore to be the more distally formed band-ogive foliation, which becomes distorted near the terminus as ice approaches the adverse slope and frontal

moraine. Debris bands therefore appear to be consistent with thrusting along band-ogive parallel foliation due to longitudinal ice flow compression (cf. Swift et al., 2006).

At Kvíárjökull, ogive-parallel foliation and the resultant debris bands are glacier-wide (Swift et al., 2006), meaning the shorter nature of the bands at Svínafellsjökull is curious. Because thrusting on such very short distances is implausible, we suggest that the discontinuous nature of the bands reflects the availability of basal ice and debris at the point of thrust origin. A particularly strong control on basal ice and till continuity is proximity to hydraulically efficient subglacial meltwater channels. These have prodigious sediment transport capacity (e.g. Alley et al., 1997; Swift et al., 2002, 2005) and commonly occur as R-channels that melt upwards into glacier, flushing away basal debris and destroying basal ice. Further support for the presence of large subglacial channels is the abundance of large-calibre RWR clasts in particular bands, mainly in the southern part of the terminus, that indicate energetic fluvial transport. At Kvíárjökull, widespread emergence of large-calibre rounded debris in thrusts has been interpreted to reflect entrainment from a fluvial lag deposit within the overdeepening (Swift et al., 2006). However, at Svínafellsjökull, the presence of fluvial material in bands at is very localised. This indicates that bands entrain fluvial material deposited within narrow zones or 'corridors' associated with a limited number of major subglacial drainage axes.

The above evidence indicates that active thrusting (and the zone of entrainment of basal materials into thrusts) is located close to the 'normal' (i.e. downglacier-facing) slope of an overdeepening beneath the lower ablation area where (1) subglacial water fluxes are large enough for R-channel formation and (2) proximity to an adverse (i.e. upglacier-facing) bedslope sufficiently reduces the subglacial hydraulic gradient to cause deposition of large-calibre fluvial material along major drainage routes (cf. Röthlisberger and Lang, 1987). Limited radar survey data indicates a c. 6 km long overdeepening extending upglacier from the terminus (Fig. 1c), meaning the most prominent normal slope lies immediately downglacier of the ice fall and therefore too close to the ELA (Fig. 1c) for subglacial water fluxes to be high. Nonetheless, the transverse crevasse field located between ~2.25 and ~3.5 km from the terminus (Fig. 11), which indicates longitudinally extending flow, means a further prominent normal slope must exist at this point. It is therefore most likely that basal materials are entrained into thrusts as ice flow enters a separate, terminal overdeepening.

An alternative hypothesis of entrainment of large-calibre from an interglacial or early-to mid-Holocene beach or glaciofluvial deposit situated below the glacier, which has been promoted as a possible origin for well-rounded gravels found in thrust structures and moraine mounds at Brøggerhalvøya, Spitsbergen (Huddart et al., 1998; Glasser et al., 1999), is also appealing. However, this is considered less likely because such a deposit would be quite extensive, and, as a consequence, the occurrence of large-calibre material in debris bands would be widespread.

5.2. Basal ice formation

In 2005, 2007, basal ice facies reflected an upper, dispersed facies overlying stratified and stratified solid facies. Previous analysis of isotope data (Cook et al., 2011a) concluded that dispersed facies ice was a far-travelled mixture of englacial and regelation basal ice as a result of basal ice being elevated by deformation at the base of the ice fall.

Assuming that englacial ice is the dominant melt source, isotope data show that crevasse-fill samples, and those of several stratified and stratified solid ice samples, had isotope compositions consistent with freezing under open-system conditions (i.e. where the melt source was constantly replenished) (cf. Cook et al., 2010). Of these samples, the crevasse-fill group all exhibited either vertically inclined layering, as observed on Survey 3, or 'herringbone'-like textures, as observed on Survey 2. The fine debris and laminae of the two 'stratified' ice samples that exhibited a supercooling-consistent offset (Survey 2, samples BB and BG) also indicates these were herringbone-like crevasse-fill features, formed relatively near the ice margin, that had then been subjected to strain-induced deformation. Two stratified solid samples (Survey 1) also exhibited a supercooling offset, though two further samples of the same material did not.

Other sampled basal ice types were also insufficiently offset to be consistent with open-system freezing. Dispersed and stratified sample compositions instead appeared to follow a lower gradient refreezing line than expected for open-system refreezing, meaning dispersed, debris-band and stratified samples were more consistent with a closed-system process, for example regelation (Jouzel and Souchez, 1982). However, stratified facies observed at the terminus occurred in thick exposures inconsistent with a simple regelation origin. The additional thickness is partly explained by observations of folds that indicate tectonic thickening of the basal ice layer. Further, the contiguous nature of layering in stratified basal ice and diamicton below on survey 1, indicates that relatively thick (10s of cm) sequences of stratified ice may form by freeze-on of water from a saturated till layer. Size analyses of stratified ice and diamicton supports freeze-on of water from the diamicton — rather than deposition of the diamicton by melt-out from basal ice layers — because stratified ice is deficient in <32 μm material relative to the diamicton. This is consistent with laboratory controlled freezing experiments (e.g. Hubbard, 1991; Cook et al., 2012) and vertical regelation studies (Iverson, 1993; Iverson and Semmens, 1995) that indicate favourable entrainment of coarser sediment.

Stratified solid facies was also observed in thick sequences, but at its thickest (e.g. survey 3) was not obviously thickened by folding, instead exhibiting quasi-bed parallel layers. Clasts sampled from this facies were less rounded and striated than clasts from diamicton samples, indicating that stratified solid facies debris had travelled a shorter distance in active transport than the diamicton. This facies was considered by Cook et al. (2007, 2010) to be consistent with a supercooling origin due to resemblance with the 'Solid' facies of Lawson (1979), which has since been attributed to supercooling by Lawson et al. (1998). Cook et al. (2007, 2010) observed this and other facies attributable to supercooling only in the southern region of the terminus, where there was also direct evidence of upwelling of supercooled subglacial waters. Limited isotope analyses presented here (four samples from survey 1) confirm that, compositionally, this facies is not fully consistent with a fully open-system freezing context. Instead, the thin, debris rich and clean ice laminae appear to indicate incremental freezing of mm-thick, occasionally highly sediment-laden water films characteristic of a hydraulically inefficient basal drainage system. Freeze-on in this environment might occur by freezing of free-flowing water films or via a combination of regelation infiltration and segregation ice formation, as proposed by Christoffersen and Tulaczyk (2003) and Christoffersen et al. (2006).

The above discussion indicates that some stratified (but not stratified solid) ice is formed by regelation and is present in debris bands that entrain basal materials before ice reaches the adverse slope of the overdeepening. Larger quantities of stratified and then stratified solid facies are then accreted near-to or on the adverse slope of the overdeepening, where conditions tend toward supercooling and hydrological connectivity at the ice-bed interface varies strongly as a result of subglacial slope and proximity to major subglacial drainage axes. At the northern region of the frontal margin, debris-poor stratified facies with compositions reflective of
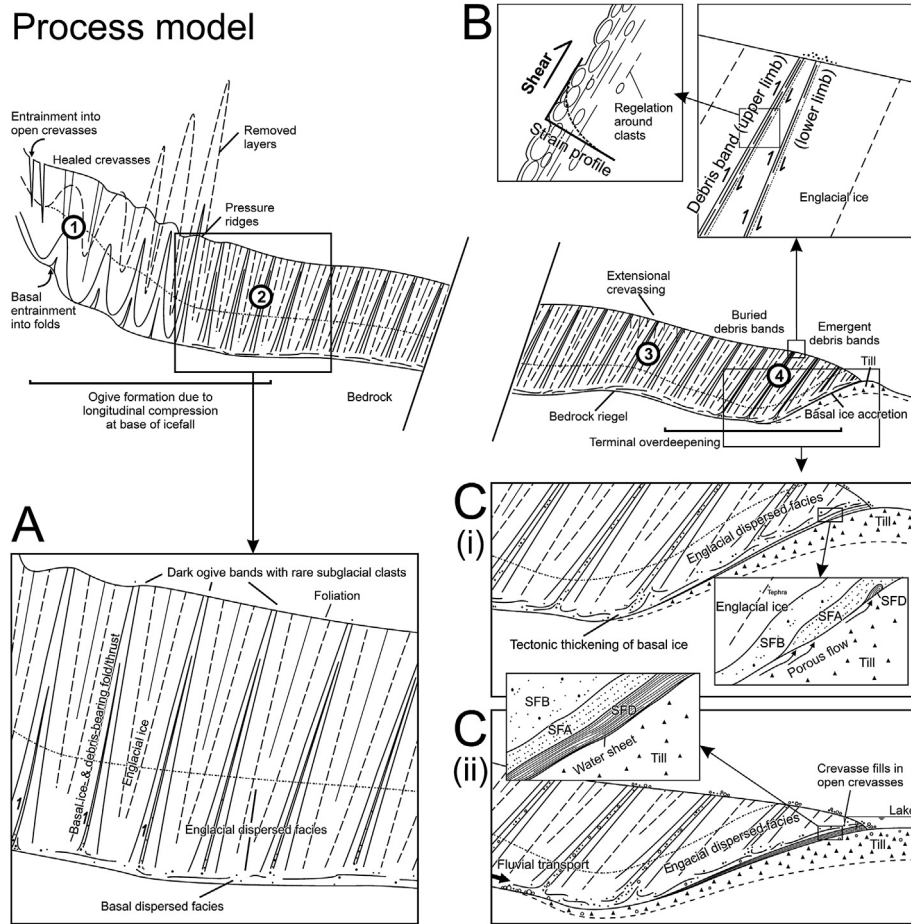
Fig. 17. Process model illustrating the key proposed debris-rich glacial ice formation processes, debris transport pathways, and glaciological controls. 1. Entrainment into basal folds and surface crevasses at the ice fall. 2. Deformation below the ice fall further elevates basal material into dark-ogive bands (see detail in panel A). 3. Ice and subglacial water flow enters the terminal overdeepening. 4. Longitudinal flow compression produces thrusting along ogive-band foliation, whilst ablation reveals some closely spaced bands that may represent separate fold arms inherited from open folds formed at the base of the icefall (see detail in panel B). Steeper adverse slopes are less connected hydrologically and basal ice facies reflect near-closed refreezing conditions (panel Ci). Major axes of subglacial water flow are directed toward the deepest areas of overdeepening, where pressurisation of flow causes coarse material in fluvial transport to be deposited on the normal slope, which is then entrained into thrusts and basal ice. Shallower adverse slopes are more connected hydrologically and ice facies reflect more open water flow and refreezing conditions, including sheets, canals and channels (panel Cii). For key to facies codes see Table 1.

near-closed refreezing conditions were dominant, indicating distributed basal hydrology characterised by limited system transmissivity and low subglacial water fluxes. Stratified solid facies with compositions reflective of more open refreezing conditions occur in the southern region, where they indicate higher transmissivity — though still distributed — flow associated with higher water fluxes and higher rates of sediment mobilisation.

Finally, a subpopulation of dispersed samples lying close to the meteoric water line, and overlapping with englacial samples, indicates two types of dispersed facies: a stratigraphically lower facies with a debris colour and clast character consistent with that of stratified basal ice and subglacial diamicton, which is interpreted as a basally derived facies, and an upper facies with dominantly angular tephra debris, which is interpreted as an englacially formed facies.

5.3. Process model and implications

5.3.1. Process model

Fig. 17 illustrates the key debris-rich ice formation processes and debris transport pathways at Svínafellsjökull and their glaciological controls. In the upper glacier tongue, deformation within the icefall disperses supraglacial debris that enters supraglacial crevasses into low-level glacial ice, and at the base of the ice fall (Figs. 17 and 1) imparts cross-glacier arcuate band-type ogive foliation that elevates basal ice and debris into basal folds, the upper limbs of which develop into thrusts (cf. Goodsell et al., 2002; Swift et al., 2006). Internal deformation then causes rotation of ogive foliation, and particularly high strain rates near the bed disperse basal ice and debris to form a relatively thick dispersed facies basal ice layer (Figs. 17 and 2) (cf. Cook et al., 2011a). Surface ablation slowly exhumes buried englacial structures, including fold limbs and blind thrusts, during flow of ice toward the terminus. The centre supraglacial sample (Fig. 15c) confirms that ogive formation is associated with some basal material being elevated to the surface. Observation of pairs of bands, where the downglacier band is steeper, indicate that bands are comprised of two fold 'arms', with shearing later taking place along each arm, and both fold arms only visible close to the terminus where ablation has exposed them.

In the lower glacier tongue, subglacial drainage forms an efficient channelized drainage system, and extending flow occurs as ice enters a terminal overdeepening (Figs. 17 and 3). However, within the overdeepening, the proximity of the adverse slope causes the subglacial hydraulic gradient to decrease and a switch from longitudinal flow extension to compression. The former results in the deposition of coarse material near to major drainage
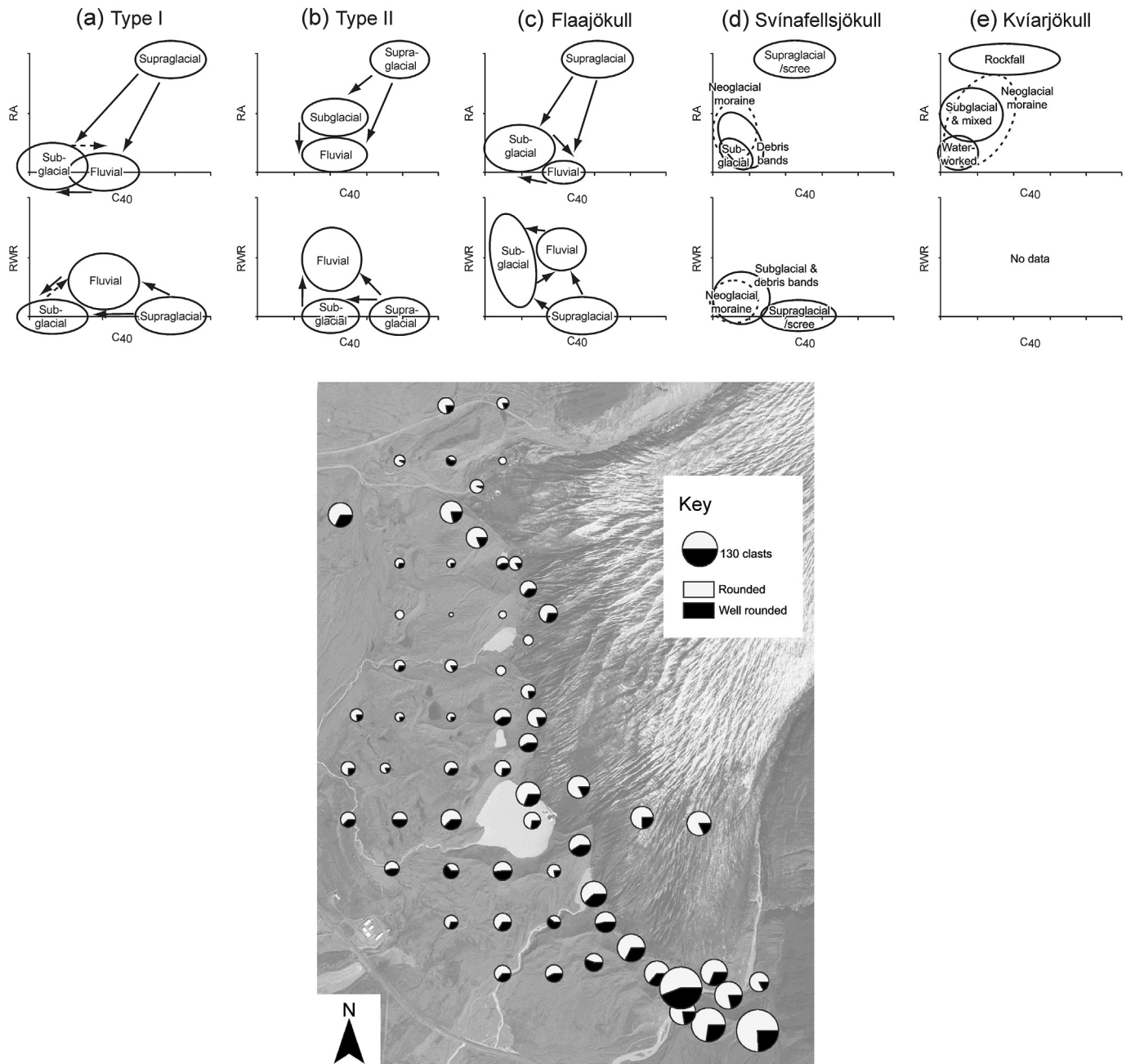
Fig. 18. Above: Clast form co-variance summary plots. (a) and (b): Two main co-variance types identified by Lukas et al. (2013) from a large temperate glacier dataset (Type I: mountain glaciers; Type II: high-mountain glaciers). (c): Co-variance plots for Flaajökull showing a higher proportion of RWR clasts in subglacial origin sediments than is typical arising from transfers of material between subglacial and fluvial transport paths (Lukas et al., 2013). (d): Co-variance plots for Svínafellsjökull showing a less substantial but still marked proportion of RWR clasts in subglacial origin material and frontal moraines. Frontal moraine characteristics overlap notably with debris band characteristics. (e): Co-variance plot for Kvíárjökull redrawn from Spedding and Evans (2002) showing similar overlap between frontal moraine and 'water-worked' supraglacial material derived from englacial channel fill and debris-band melt out (cf. Swift et al., 2006). Below: Abundance of RWR clasts in the frontal moraine system at Svínafellsjökull determined by sampling of all surface clasts in a 25 m² grid. Symbol size is proportional to clast count and shows relative proportion of rounded and well-rounded clasts.

axes on the normal slope of the overdeepening, whilst the latter reactivates ogive-origin englacial fold and thrust structures that entrain basal materials (Figs. 17 and 4). Eventual distribution of water across the bed will encourage till accumulation on the adverse slope (cf. Hooke, 1991) and ultimately the deposition of a large proportion of the fluvial sediment load, and may be accompanied by glaciohydraulic supercooling. This results in the high incidence of RWR clasts within thrusts and basal ice more generally. The geometry of the overdeepening directs the majority of

subglacial water flow toward the deeper southern region of the terminus. This causes near-closed freezing conditions to dominate in the northern region of the terminus, leading to predominantly stratified facies formation, whereas more open, possibly sheet flow, conditions dominate in some areas of the southern region, forming stratified solid ice.

It is of course possible that high confining pressures means thrusts originate at depth as folds (cf. Moore et al., 2011), with slip being initiated only near the glacier surface or in thinner ice near

the terminus (cf. Moore et al., 2010). Observation of pairs of bands, with a steeper downglacier band, may be indicative of bands originating via open folds beneath the ice fall (cf. Swift et al., 2006), and thus comprising two distinct fold 'arms', with thrusting that reaches the surface taking place later, where ice is thinner, on one or both arms. The possibility that persistently high water pressures within the overdeepening may be critical in forming and maintaining basal fractures that are exploited as thrust planes (cf. Moore et al., 2010) should also be considered.

5.3.2. Significance and implications

Glaciohydraulic supercooling plays a key role in the evolution of glacier bed morphology (Alley et al., 2003). In the Alley et al. (2003) model, an adverse slope that meets the supercooling threshold (i.e. 1.2 to 1.7 times the ice surface slope) will cause supercooling within subglacial channels to curtail the ability of subglacial water to transport basal sediment. Under such circumstances, some sediment may be removed by freeze-on to the glacier base in the form of debris-rich stratified facies basal ice (e.g. Alley et al., 1998; Lawson et al., 1998; Cook et al., 2007, 2010), but most sediment will be deposited. Central to this model is the notion that supercooling and basal ice formation is focussed within large channels that results in largely open-system isotope compositions. At Svínafellsjökull, basal ice formation is pervasive, and the geometry of the overdeepening leads to a wide range of conditions and ice types that do not necessarily reflect open-system refreezing. Further, it is because refreezing is not limited to channels that debris-rich basal ice is so varied and prevalent.

Sediment transfer at Svínafellsjökull is not confined to basal ice formation, and includes substantial entrainment of subglacial and fluvial material along thrusts. Similar complexity of transfer pathways, involving apparent transfer between the fluvial and subglacial realm, have been inferred from proglacial clast analysis at many Icelandic glaciers, including Flaajökull (Lukas et al., 2013), Skalafellsjökull (Evans, 2000), and Kvíárjökull (Spedding and Evans, 2002), and are not therefore isolated examples (Fig. 18), but are presently underappreciated in landscape evolution models (e.g. Alley et al., 2003). Proglacial clast data at Svínafellsjökull and Kvíárjökull (Fig. 18) indicates that these processes are important in providing sediment for moraine formation and that englacial thrusting is therefore, temporally and spatially, a pervasive transport mechanism that is significant in terms of its volume. Notably, mean proglacial clast form characteristics at Svínafellsjökull (Figs. 15 and 16) are closest to debris bands and their associated supraglacial moraines than clasts within stratified basal ice layers. The prevalence of thrusting as a means of debris transfer therefore needs to be considered, particularly within overdeepened glacier systems, where it seems likely to be important for rates and processes of landscape evolution (Cook and Swift, 2012; cf. Alley et al., 2003).

Finally, because overdeepenings are common beneath glaciers and ice sheets, our observations indicate that thrusting as a significant means of ice flow and sediment transfer is not restricted to surging and polythermal glaciers, as has sometimes been assumed. Glacier flow models therefore need to incorporate the potential for englacial thrusting on glacier-thickness scales where there are adverse slopes. The siting of geological facilities for long-term nuclear waste disposal in regions that may be affected by future glaciation (e.g. Talbot, 1999; Fischer and Haeberli, 2010; Iverson and Person, 2012; Fischer et al., 2014) may also need to consider such processes because thrusts appear able to entrain material from areas of deep erosion at the glacier bed, concentrating it in surface structures.

6. Conclusion

Understanding of the potential complexity of glacial debris transfer pathways is important if we are to fully understand the overall capacity of glacial transport systems and their implications for glacial landscape evolution and the Quaternary record. Our study of Svínafellsjökull indicates that a large number of active transport pathways are present, and that mixing of debris between transport pathways is significant. The overall picture is influenced very strongly by the presence of a terminal overdeepening, which promotes deposition of sediment from subglacial fluvial transport pathways, inhibits the flushing of subglacial sediment by fluvial processes, promotes the formation of thick sequences of basal ice that may be thickened tectonically by flow along the adverse slope, and promotes active transport of basal ice and debris to the glacier surface along thrust planes. Overdeepenings are common beneath glaciers and ice sheets, meaning potential for thrusting as a significant means of transfer is not restricted to surging and polythermal glaciers, as has been assumed. Further, tectonic processes appear to play a key role in maintaining continuity of sediment transfer through overdeepenings. Finally, we suggest that glacier flow models need to incorporate the potential for englacial thrusting on glacier-thickness scales where there are adverse slopes.

Evidence of thrusting at Svínafellsjökull, as at Kvíárjökull (Swift et al., 2006), is persuasive and therefore a plausible and pervasive transfer process in temperate glaciers. Criteria for identifying thrusts will likely remain subject to debate, but we provide several observations that indicate key diagnostic processes; specifically, (a) simple shear along the upper surface of the band, resulting in entrainment of material into and along the band by traction and the development of a strong clast-rich fabric in this layer; and (b) straining of material within and below the band, in which the depth of deformation and resultant mixing of band and englacial ice is dependent on ice properties and the proportion of movement accommodated by simple shear. This dual mechanism explains how bands achieved thicknesses of several decimetres, rather than being limited to mm-thick shear planes containing debris-rich ice associated with regelation-layer thicknesses. Weaknesses in glacier structure (e.g. dark ogive foliation; Swift et al., 2006) nevertheless appear to be required for thrusting to occur (cf. Moore et al., 2010), and these weaknesses determine the precise location and extent of thrust occurrence.

Debris transfer by basal ice formation is also significant. The origin of basal ice has been subject to much debate concerning the significance of glaciohydraulic supercooling because the composition of many ice types at Svínafellsjökull and elsewhere is not consistent with fully open system refreezing conditions that would be characteristic of hydrologically well-connected arterial subglacial channels. Such channels likely exist upglacier of the overdeepening, where they will destroy basal ice and flush basal sediment into the overdeepening. Within the overdeepening, however, water will distribute across the bed. Thus, we propose that the hydrological connectivity of the bed dictates basal ice formation rates and processes, resulting in a range of facies types and compositions in different locations along the margin. Notably, stratified facies that are consistent with near-closed conditions is present in thick sequences in the northern region of the terminus and appears to reflect freeze-on of water directly from water flow within a subglacial diamicton layer. Only in the southern region, which appears to be the main route for water flow, does debris-rich ice form that is consistent with freezing in more open flow conditions, though still apparently within a broad sheet.

Acknowledgements

Appendix A. Supplementary data

Supplementary data related to this article can be found at https://doi.org/10.1016/j.quascirev.2017.11.027.

References

Alley, R.B., Cuffey, K.M., Evenson, E.B., Strasser, J.C., Lawson, D.E., Larson, G.J., 1997. How glaciers entrain and transport basal sediment: physical constraints. Quat. Sci. Rev. 16, 1017–1038.

Alley, R.B., Lawson, D.E., Evenson, E.B., Strasser, J.C., Larson, G.J., 1998. Glaciohydraulic supercooling: a freeze-on mechanism to create stratified, debris-rich basal ice: II. Theory. J. Glaciol. 44, 563–569.

Alley, R.B., Lawson, D.E., Larson, G.J., Evenson, E.B., Baker, G.S., 2003. Stabilizing feedbacks in glacier-bed erosion. Nature 424, 758–760.

Benn, D.I., 2004. Clast morphology. In: Evans, D.J.A., Benn, D.I. (Eds.), A Practical Guide to the Study of Glacial Sediments. Arnold, London.

Bennett, G.L., Evans, D.J.A., 2012. Glacier retreat and landform production on an overdeepened glacier foreland: the debris-charged glacial landsystem at Kvíárjökull. Icel. Earth Surf. Process. Landforms 37, 1584–1602.

Bennett, M.R., Waller, R.I., Glasser, N.F., Hambrey, M.J., Huddart, D., 1999. Glacigenic clast fabrics: genetic fingerprint or wishful thinking? J. Quat. Sci. 14, 125–135.

Christoffersen, P., Tulaczyk, S., 2003. Response of subglacial sediments to basal freeze-on: I. Theory and comparison to observations from beneath the West Antarctic ice sheet. J. Geophys. Res. 108 (B4), 2222.

Christoffersen, P., Tulaczyk, S., Carsey, F., Behar, A.E., 2006. A quantitative framework for interpretation if 428 basal ice facies formed by ice accretion over subglacial sediment. J. Geophys. Res. 111 (F1), F01017.

Cook, S.J., 2006. The Role of Glaciohydraulic Supercooling in the Formation of Stratified Facies Basal Ice. Unpublished PhD thesis. Keele University.

Cook, S.J., Swift, D.A., 2012. Subglacial basins: their origin and importance in glacial systems and landscapes. Earth Sci. Rev. 115, 332–372.

Cook, S.J., Knight, P.G., Waller, R.I., Robinson, Z.P., Adam, W.G., 2007. The geography of basal ice and its relationship to glaciohydraulic supercooling: Svínafellsjökull, southeast Iceland. Quat. Sci. Rev. 26, 2309–2315.

Cook, S.J., Robinson, Z.P., Fairchild, I.J., Knight, P.G., Waller, R.I., Boomer, I., 2010. Role of glaciohydraulic supercooling in the formation of stratified facies basal ice: Svínafellsjökull and Skaftafellsjökull, southeast Iceland. Boreas 39, 24–38.

Cook, S.J., Swift, D.A., Graham, D.J., Midgley, N.G., 2011a. Origin and significance of 'dispersed facies' basal ice: Svínafellsjökull, Iceland. J. Glaciol. 57, 710–720.

Cook, S.J., Graham, D.J., Swift, D.A., Midgley, N.G., Adam, W.G., 2011b. Sedimentary signatures of basal ice formation and their preservation in ice-marginal sediments. Geomorphology 125, 122–131.

Cook, S.J., Knight, P.G., Knight, D.A., Waller, R.I., 2012. Laboratory experiments of sediment entrainment by freezing supercooled water. Geogr. Ann. Ser. A Phys. Geogr. 94, 351–362.

Creyts, T.T., Clarke, G.K.C., 2010. Hydraulics of subglacial supercooling: theory and simulations for clear water flows. J. Geophys. Res. Earth Surf. 115 (F3), F03021.

Egholm, D.L., Pedersen, V.K., Knudsen, M.F., Larsen, N.K., 2012. Coupling the flow of ice, water, and sediment in a glacial landscape evolution model. Geomorphology 141–142, 47–66.

Ensminger, S.L., Alley, R.B., Evenson, E.B., Lawson, D.E., Larson, G.J., 2001. Basal-crevasse-fill origin of laminated debris bands at Matanuska Glacier, Alaska, USA. J. Glaciol. 47, 412–422.

Evans, D.J.A., 2000. A gravel outwash/deformation till Continuum, Skalafellsjokull, Iceland. Geogr. Ann. Phys. Geogr. 82, 499–512. https://doi.org/10.1111/j.0435-3676.2000.00137.x.

Evans, D.J.A., 2003. Glacial Landsystems. Hodder Arnold.

Evans, D.J.A., 2009. Controlled moraines: origins, characteristics and palaeoglaciological implications. Quat. Sci. Rev. 28, 183–208.

Fischer, U.H., Haeberli, W., 2010. Glacial Erosion Modelling: Results of a Workshop Held in Unterägeri, Switzerland, 29 April – 1 May 2010. Nationale Genossenschaft für die Lagerung radioaktiver Abfälle (National Cooperative for the Disposal of Radioactive Waste), Hardstrasse 73, CH-5430 Wettingen, Switzerland. Arbeitsbericht NAB 10–34.

Fischer, U.H., Bebiolka, A., Brandefelt, J., Follin, S., Hirschorn, S., Jensen, M., Keller, S., Kennel, L., Näslund, J.-O., Normani, S., Selroos, J.-O., Vidstrand, R., 2014. Radioactive waste under conditions of future ice ages. In: In, Haeberli W., Whiteman, C. (Eds.), Snow and Ice-related Hazards, Risks and Disasters. Elsevier, Amsterdam, pp. 345–393.

Fountain, A.G., Walder, J.S., 1998. Water flow through temperate glaciers. Rev. Geophys. 36, 299–328.

Glasser, N.F., Bennett, M.R., Huddart, D., 1999. Distribution of glaciofluvial sediment within and on the surface of a high arctic valley glacier: marthabreen, Svalbard. Earth Surf. Process. Landforms 24, 303–318.

Glasser, N.F., Hambrey, M.J., Etienne, J.L., Jansson, P., Pettersson, R., 2003. The origin and significance of debris-charged ridges at the surface of Storglaciären, northern Sweden. Geogr. Ann. Ser. A Phys. Geogr. 85, 127–147.

Goodsell, B., Hambrey, M.J., Glasser, N.F., 2002. Formation of band ogives and associated structures at Bas Glacier d'Arolla, Valais, Switzerland. J. Glaciol. 48, 287–300.

Graham, D.J., Midgley, N.G., 2000. Graphical representation of particle shape using triangular diagrams: an Excel spreadsheet method. Earth Surf. Process. Landforms 25, 1473–1477.

Graham, D.J., Bennett, M.R., Glasser, N.F., Hambrey, M.J., Huddart, D., Midgley, N.G., 2007. A test of the englacial thrusting hypothesis of "hummocky" moraine formation: case studies from the northwest Highlands, Scotland (Comment). Boreas 36, 103–107.

Hambrey, M.J., Glasser, N.F., 2012. Discriminating glacier thermal and dynamic regimes in the sedimentary record. Sediment. Geol. 251–252, 1–33.

Hambrey, M.J., Dowdeswell, J.A., Murray, T., Porter, P.R., 1996. Thrusting and debris entrainment in a surging glacier: bakaninbreen, Svalbard. Ann. Glaciol. 22, 241–248.

Hambrey, M.J., Huddart, D., Bennett, M.R., Glasser, N.F., 1997. Genesis of 'hummocky moraines' by thrusting in glacier ice: evidence from Svalbard and Britain. J. Geol. Soc. 154, 623–632.

Hambrey, M.J., Bennett, M.R., Dowdeswell, J.A., Glasser, N.F., Huddart, D., 1999. Debris entrainment and transfer in polythermal valley glaciers. J. Glaciol. 45, 69–86.

Hannesdóttir, H., Björnsson, H., Pálsson, F., Aðalgeirsdóttir, G., Guðmundsson, S., 2015. Changes in the southeast Vatnajökull ice cap, Iceland, between 1890 and 2010. Cryosphere 9, 565–585.

Hicock, S.R., 1991. On subglacial Stone pavements in till. J. Geol. 99, 607–619.

Hooke, R.L., 1991. Positive feedbacks associated with erosion of glacial cirques and overdeepenings. Geol. Soc. Am. Bull. 103, 1104–1108.

Hooke, R.LeB., Hudleston, P.J., 1978. Origin of foliation in glaciers. J. Glaciol. 20, 285–299.

Hubbard, B., 1991. Freezing-rate effects on the physical characteristics of basal ice formed by net adfreezing. J. Glaciol. 37, 339–347.

Hubbard, B., Sharp, M., 1989. Basal ice formation and deformation: a review. Prog. Phys. Geogr. 13, 529–558.

Hubbard, B., Sharp, M.J., 1993. Weertman regelation, multiple refreezing events and the isotopic evolution of the basal ice layer. J. Glaciol. 39, 275–291.

Hubbard, B., Tison, J., Janssens, L., Spiro, B., 2000. Ice-core evidence of the thickness and character of clear-facies basal ice: glacier de Tsanfleuron, Switzerland. J. Glaciol. 46, 140–150.

Hubbard, B., Glasser, N., Hambrey, M., Etienne, J., 2004. A sedimentological and isotopic study of the origin of supraglacial debris bands: kongsfjorden, Svalbard. J. Glaciol. 50, 157–170.

Hubbard, B., Cook, S., Coulson, H., 2009. Basal ice facies: a review and unifying approach. Quat. Sci. Rev. 28, 1956–1969.

Huddart, D., Bennett, M.R., Hambrey, M.J., Glasser, N.F., Crawford, K., 1998. Origin of well-rounded gravels in glacial deposits from Brøggerhalvøya, northwest Spitsbergen: potential problems caused by sediment reworking in the glacial environment. Polar Res. 17, 61–69.

Iverson, N.R., 1993. Regelation of ice through debris at glacier beds: implications for sediment transport. Geology 21, 559–562.

Iverson, N., Person, M., 2012. Glacier-bed geomorphic processes and hydrologic conditions relevant to nuclear waste disposal. Geofluids 12, 38–57.

Iverson, N.R., Semmens, D.J., 1995. Intrusion of ice into porous media by regelation: a mechanism of sediment entrainment by glaciers. J. Geophys. Res. 100 (B7), 10219–10230.

Jouzel, J., Souchez, R.A., 1982. Melting-refreezing at the glacier sole and the isotopic composition of the ice. J. Glaciol. 28, 35–42.

King, C.A.M., Ives, J.D., 1956. Glaciological observations on some of the outlet glaciers of south-west Vatnajökull, Iceland, 1954. Part II: Ogives. J. Glaciol. 2, 646–651.

Knight, P.G., 1987. Observations at the edge of the Greenland ice sheet: Boundary condition implications for modellers. In: Symposium at Vancouver 1987-The Physical Basis of Ice Sheet Modelling. IAHS Publ. 170, pp. 359–366.

Knight, P.G., 1994. Two-facies interpretation of the basal layer of the Greenland ice sheet contributes to a unified model of basal ice formation. Geology 22, 971–974.

Knight, P.G., 1997. The basal ice layer of glaciers and ice sheets. Quat. Sci. Rev. 16, 975–993.

Knight, P.G., Sugden, D.E., Minty, C.D., 1994. Ice flow around large obstacles as indicated by basal ice exposed at the margin of the Greenland ice sheet. J. Glaciol. 40, 359—367.

Knighton, D., 1998. Fluvial Forms and Processes: a New Perspective. Arnold, London.

Krüger, J., 1994. Glacial processes, sediments, landforms, and stratigraphy in the terminus region of Myrdalsjökull, Iceland. Folia Geogr. Danica 21, 1—233.

Larson, G.J., Lawson, D.E., Evenson, E.B., Knudsen, O., Alley, R.B., Phanikumar, M.S., 2010. Origin of stratified basal ice in outlet glaciers of Vatnajökull and Oræfajökull. Icel. Boreas 39, 459—470.

Lawson, D.E., 1979. Sedimentological Analysis of the Western Terminus Region of the Matanuska Glacier, Alaska. Cold Regions Research and Engineering Laboratory. Report 79-9, 6—27.

Lawson, D.E., Strasser, J.C., Evenson, E.B., Alley, R.B., Larson, G.J., Arcone, S.A., 1998. Glaciohydraulic supercooling: a freeze-on mechanism to create stratified, debris-rich basal ice: I. Field evidence. J. Glaciol. 44, 547—562.

Lovell, H., Fleming, E.J., Benn, D.I., Hubbard, B., Lukas, S., Naegeli, K., 2015. Former dynamic behaviour of a cold-based valley glacier on Svalbard revealed by basal ice and structural glaciology investigations. J. Glaciol. 61, 309—328.

Lukas, S., 2005. A test of the englacial thrusting hypothesis of 'hummocky' moraine formation: case studies from the northwest Highlands, Scotland. Boreas 34, 287—307.

Lukas, S., Benn, D.I., Boston, C.M., Brook, M.S., Coray, S., Evans, D.J.A., Graf, A., Kellerer-Pirklbauer-Eulenstein, A., Kirkbride, M.P., Krabbendam, M., Lovell, H., Machiedo, M., Mills, S.C., Nye, K., Reinardy, B.T.I., Ross, F.H., Signer, M., 2013. Clast shape analysis and clast transport paths in glacial environments: a critical review of methods and the role of lithology. Earth-Sci. Rev. 121, 96—116.

Magnússon, E., Pálsson, F., Björnsson, H., Guðmundsson, S., 2012. Removing the ice cap of Öræfajökull central volcano, SE-Iceland: mapping and interpretation of bedrock topography, ice volumes, subglacial troughs and implications for hazards assessments. Jökull 62, 132—150.

Moore, P.L., Iverson, N.R., Cohen, D., 2010. Conditions for thrust faulting in a glacier. J. Geophys. Res. 115, F02005.

Moore, P.L., Iverson, N.R., Brugger, K.A., Cohen, D., Hooyer, T.S., Jansson, P., 2011. Effect of a cold margin on ice flow at the terminus of Storglaciären, Sweden: implications for sediment transport. J. Glaciol. 57, 77—87.

Phillips, E., Everest, J., Evans, D.J.A., Finlayson, A., Ewertowski, M., Guild, A., Jones, L., 2017. Concentrated, 'pulsed' axial glacier flow: structural glaciological evidence from Kvíárjökull in SE Iceland. Earth Surf. Process. Landforms 42, 1901—1922.

https://doi.org/10.1002/esp.4145.

Powers, M.C., 1953. A new roundness scale for sedimentary particles. J. Sediment. Petrol. 23, 117—119.

Roberts, M.J., Tweed, F.S., Russell, A.J., Knudsen, O., Lawson, D.E., Larson, G.J., Evenson, E.B., Björnsson, H., 2002. Glaciohydraulic supercooling in Iceland. Geology 30, 439—442.

Röthlisberger, H., Lang, H., 1987. Glacial hydrology. In: Gurnell, A.M., Clark, M.J. (Eds.), Glacio-fluvial Sediment Transfer; an Alpine Perspective. New York, Etc. John Wiley and Sons, pp. 207—284.

Sharp, M.J., Jouzel, J., Hubbard, B., Lawson, W., 1994. The character, structure and origin of the basal ice layer of a surge-type glacier. J. Glaciol. 40, 327—340.

Spedding, N., Evans, D.J.A., 2002. Sediments and landforms at Kvíárjökull, southeast Iceland: a reappraisal of the glaciated valley landsystem. Sediment. Geol. 149, 21—42.

Sugden, D.E., Marchant, D.R., Lorrain, R., Tison, J.-L., Jouzel, J., 1987. Evidence for two zones of debris entrainment beneath the Greenland ice sheet. Nature 328, 238—241.

Swift, D.A., 2011. Basal Sediment Evacuation by Subglacial Drainage Systems. Encyclopedia of Snow, Ice and Glaciers. Springer, pp. 85—90.

Swift, D.A., Nienow, P.W., Spedding, N., Hoey, T.B., 2002. Geomorphic implications of subglacial drainage configuration: rates of basal sediment evacuation controlled by seasonal drainage system evolution. Sediment. Geol. 149, 5—19.

Swift, D.A., Nienow, P.W., Hoey, T.B., Mair, D.W.F., 2005. Seasonal evolution of runoff from Haut Glacier d'Arolla, Switzerland and implications for glacial geomorphic processes. J. Hydrol. 309, 133—148.

Swift, D.A., Evans, D.J.A., Fallick, A.E., 2006. Transverse englacial debris-rich ice bands at Kvíárjökull, southeast Iceland. Quat. Sci. Rev. 25, 1708—1718.

Talbot, C.J., 1999. Ice ages and nuclear waste isolation. Eng. Geol. 52, 177—192.

Toubes-Rodrigo, M., Cook, S.J., Elliott, D., Sen, R., 2016. Sampling and describing glacier ice. In: Cook, S.J., Clarke, L.E., Nield, J. (Eds.), Geomorphological Techniques. British Society for Geomorphology, London.

Weertman, J., 1961. Mechanism for the formation of inner moraines found near the edge of cold ice caps and ice sheets. J. Glaciol. 3, 965—978.

Woodward, J., Murray, T., McCaig, A., 2002. Formation and reorientation of structure in the surge-type glacier Kongsvegen, Svalbard. J. Quat. Sci. 17, 201—209.

Woodward, J., Murray, T., McCaig, A., 2003. Reply to Glasser et al., 2003. J. Quat. Sci. 18, 99—100.